Original Article

MOLECULAR METABOLISM

Metformin overcomes metabolic reprogramming-induced resistance of skin squamous cell carcinoma to photodynamic therapy

Marta Mascaraque-Checa [1,2], María Gallego-Rentero [1,2], Jimena Nicolás-Morala [1,2], Mikel Portillo-Esnaola [1,2], José M. Cuezva [3], Salvador González [4], Yolanda Gilaberte [5], Ángeles Juarranz [1,2,*]

ABSTRACT

Objective: Cancer metabolic reprogramming promotes resistance to therapies. In this study, we addressed the role of the Warburg effect in the resistance to photodynamic therapy (PDT) in skin squamous cell carcinoma (sSCC). Furthermore, we assessed the effect of metformin treatment, an antidiabetic type II drug that modulates metabolism, as adjuvant to PDT.

Methods: For that, we have used two human SCC cell lines: SCC13 and A431, called parental (P) and from these cell lines we have generated the corresponding PDT resistant cells (10GT).

Results: Here, we show that 10GT cells induced metabolic reprogramming to an enhanced aerobic glycolysis and reduced activity of oxidative phosphorylation, which could influence the response to PDT. This result was also confirmed in P and 10GT SCC13 tumors developed in mice. The treatment with metformin caused a reduction in aerobic glycolysis and an increase in oxidative phosphorylation in 10GT sSCC cells. Finally, the combination of metformin with PDT improved the cytotoxic effects on P and 10GT cells. The combined treatment induced an increase in the protoporphyrin IX production, in the reactive oxygen species generation and in the AMPK expression and produced the inhibition of AKT/mTOR pathway. The greater efficacy of combined treatments was also seen *in vivo*, in xenografts of P and 10GT SCC13 cells.

Conclusions: Altogether, our results reveal that PDT resistance implies, at least partially, a metabolic reprogramming towards aerobic glycolysis that is prevented by metformin treatment. Therefore, metformin may constitute an excellent adjuvant for PDT in sSCC.

Keywords Skin squamous cell carcinoma; Cancer resistance; Photodynamic therapy; Warburg effect; Metformin; AKT/mTOR pathway

1. INTRODUCTION

Skin squamous cell carcinoma (sSCC) is one of the most common human malignancies, representing between 20 and 25% of all non-melanoma skin cancer cells (NMSC) [1,2]. Its incidence is continuously rising due to aging population and increased exposure to ultraviolet radiation [3–5]. The risk of metastasis is low, around 5%; however, aggressive sSCC is associated with high morbidity and mortality [6]. Alterations in PI3K (phosphatidylinositol 3-kinase) - AKT (protein kinase B) - mTOR (mammalian target of rapamycin) signaling pathway are involved in tumor progression and aggressiveness [1,7–9].

The standard treatment options for sSCC include the combination of surgery, radiotherapy and/or chemotherapy [11,12]. However, within non-invasive treatments, photodynamic therapy (PDT) stands out, since it has become one of the therapeutic modalities that has grown the most in recent years, presenting numerous advantages over other treatments. It is based on the combination of a photosensitizer (PS), light and oxygen to induce the selective death of tumor cells, by generating reactive oxygen species (ROS) [10,12–14]. One of the compounds approved for its use in oncological dermatology is methyl-aminolevulinate (MAL), a precursor of the endogenous PS protoporphyrin IX (PpIX). MAL is approved for the treatment of actinic keratosis in the U.S. and the E.U. and for *in situ* sSCC in the E.U. [15,16].

However, PDT is not always effective and recurrences may occur after the treatment [17]. Intracellular resistance mechanisms can be triggered by several causes including changes in the expression of proteins related to cell death, such as p53; activation of antioxidant defense mechanisms against ROS generation produced after PDT; and activation of cell survival pathways [18–22]. In recent years the metabolism of tumor cells has been studied as a new tumor resistance mechanism, being widely studied at chemotherapy level but not in PDT [23,24]. Otto Warburg, in 1924, observed that tumor cells, in the presence of oxygen, obtained energy through glycolysis instead of

[1]Departament of Biology, Universidad Autónoma de Madrid, Madrid, Spain [2]Instituto Ramón y Cajal de Investigaciones Sanitarias, IRYCIS, Madrid, Spain [3]Centro de Biología Molecular-Severo Ochoa (CBMSO/CSIC) and Centro de Investigación Biomédica en Red de Enfermedades Raras (CIBERER-ISCIII), Universidad Autónoma de Madrid, Madrid, Spain [4]Department of Medicine and Medical Specialties, Universidad de Alcalá, Madrid, Spain [5]Departament of Dermatología, Hospital Miguel Servet, Zaragoza, Spain

*Corresponding author. Departament of Biology, Universidad Autónoma de Madrid, Madrid, Spain. E-mail: angeles.juarranz@uam.es (Á. Juarranz).

Received October 26, 2021 • Revision received April 4, 2022 • Accepted April 5, 2022 • Available online 9 April 2022

https://doi.org/10.1016/j.molmet.2022.101496

Abbreviations

10GT	PDT resistant cell
AKT	protein kinase B
AMPK	AMP-activated protein kinase
CGH	comparative genomic hybridization
CSP	cell survival percentage
Dlog	difference in logarithms
FBS	fetal bovine serum
GAPDH	glyceraldehyde-3-phosphate dehydrogenase
GLUT	glucose transports
H&E	hematoxylin and eosin
IHC	immunohistochemically
LD20	(lethal dose of 20%)
MAL	methyl-aminolevulinate
mTOR	mammalian target of rapamycin
MTT	3-[4,5-dimethylthiazol-2-yl]-2,5-diphenyltetrazoliumbromide
NMSC	non-melanoma skin cancer
OCR	oxygen consumption rate
OSR	oligomycin sensitive respiration rate
OXPHOS	oxidative phosphorylation
P	parental
p70S6K	ribosomal protein S6 kinase β1
PBS	phosphate buffer saline
PDK1	phosphoinositide dependent kinase 1
PDT	photodynamic therapy
PET- FDG	positron emission tomography using 18-fluorodeoxyglucose
PI3K	phosphatidylinositol 3-kinase
PKM2	pyruvate kinase M2
PpIX	protoporphyrin IX
PS	photosensitizer
ROS	reactive oxygen species
SD	standard deviations
sSCC	skin squamous cell carcinoma
TUNEL	TdT-mediated dUTP nick-end labeling
WB	western blot
β-F1-ATPase	β-catalytic subunit of the mitochondrial H+-ATP synthase

using oxidative phosphorylation (OXPHOS), as occurs preferentially in differentiated (non-tumor) cells. This metabolic phenotype is called "Warburg effect". It involves a high rate of glycolysis followed by lactic acid fermentation, even in aerobic conditions, leading to the tumor acidification of the microenvironment that seems to favor tumor progression, invasion, metastasis and resistance to antitumor drugs [25–29].

There are multiple molecular mechanisms that converge to modify cellular metabolism, highlighting the role of the AKT-mTOR pathway. AKT is an important inducer of the glycolytic phenotype, increasing the expression of glucose transporters (GLUT) and stimulating mTOR activation, which plays an important role in metabolic reprogramming by increasing proliferation and biosynthesis of proteins and lipids [30–32]. In addition, it has been observed that pyruvate kinase M2 (PKM2) is highly expressed in cancer and promotes glycolysis and cell survival [33–35]. Finally, changes during the cellular metabolism reprogramming have been correlated, among other events, with a reduction of the bioenergetic index in different neoplasia. This index is related to the expression of the β-catalytic subunit of the mitochondrial H+-ATP synthase (β-F1-ATPase), which is the bottleneck of OXPHOS, to the expression of glycolytic glyceraldehyde-3-phosphate dehydrogenase (GAPDH) [36–39].

In order to improve the effectiveness of PDT, new research is being carried out in the study of the resistance mechanisms and the combination with adjuvant agents that ensure tumor eradication [14,18,40,41]. In this sense, metformin, used in type 2 diabetes mellitus, has become a promising adjuvant in oncology. The antitumorigenic role of metformin seems to be due to the fact that it interferes in metabolic reprogramming mechanisms, being one of its main targets the inhibition of mTOR, through the activation of AMPK (AMP-activated protein kinase) [42,43]. Regarding PDT, some studies have shown that metformin sensitizes and improves the response of cells to PDT with: (1) ALA in lung cancer [44], (2) phthalocyanine chloride gallium in melanoma [45], (3) 5,10,15,20-tetrakis(sulfophenyl) porphyrin, reducing angiogenesis and inflammation of Walker's carcinosarcoma [46] and (4) MAL in basal cell carcinoma [47].

For all the above, research related to the metabolism of PDT-resistant cells is of great interest and relevance for the treatment of sSCC. Furthermore, with the aim of making PDT more effective and avoiding resistance, this study evaluates the efficacy of the combination of PDT and metformin for the treatment of sSCC.

2. MATERIAL AND METHODS

2.1. Cell types

The skin squamous carcinoma cell lines (sSCC) used were SCC-13 (SCC13) [48] and A431 [49]. These cells, called parental (P), in a previous work were subjected to 10 MAL-PDT cycles to obtain resistant cells. For that, the concentration of MAL was set at 1 mM (5 h of incubation) and the red light dose was gradually increased in successive cycles to induce a survival rate lower than 20% (Supplemental Table 1) [50]. These resistant cells were inoculated in immunosuppressed mice; the induced tumors were subcultured by explants, and a cell population called 10GT was obtained (Fig. S1) [47]. The P populations, which were not inoculated in mice, and 10GT of both sSCC cell lines were grown in DMEM (Dulbecco's modified Eagle's medium high glucose) supplemented with 10% (v/v) fetal bovine serum (FBS) and 1% antibiotic (penicillin, 100 units/mL; streptomycin 100 mg/mL), all from Thermo Fisher Scientific Inc (Rockford, IL, USA). Cell cultures were performed under standard conditions of 5% CO2, 95% humidity, and 37 °C and propagated by treatment with 1 mM EDTA/0.25% Trypsin (w/v).

2.2. Spheroids (3D)

For the formation of spheroids, cells were trypsinized, centrifuged at 1800 rpm for 5 min and resuspended in spheroids medium [DMEM/F12 (1:1), 2% supplement B27 (Thermo Fisher Scientific Inc, Rockford, IL, USA), 20 ng/mL EGF, 0.4% bovine serum albumin and 4 μg/mL insulin (Sigma–Aldrich, St. Louis, MO, USA)]. Cells were then seeded at a density of 40,000 cells/mL on P6 plates covered with 1.2% poly-HEMA (2-hydroxyethyl methacrylate, Sigma–Aldrich) in 95% ethanol [51].

2.3. Treatments

The treatments were carried out when the two-dimensional cultures reached 70% confluence or the spheroids had a size around 300 μm. For PDT, methyl-aminolevulinate (MAL) (Sigma–Aldrich, St. Louis, MO, USA) was prepared at an initial concentration of 10 mM in

deionized sterile water, and the cells were incubated with 0.3 mM MAL in DMEM without FBS for 5 h in dark. Then, the cells were irradiated at variable light doses (1.5–30.4 J/cm^2) by using a red-light emitting diode source (WP7143 SURC/E Kingbright, Los Angeles, CA, USA) with an irradiance of 6.2 mW/cm^2 and an emission peak of $\lambda = 634 \pm 20$ nm. To minimize refraction of light, cells were irradiated from the bottom of the culture plates. After irradiation, the cells were incubated in DMEM with 10% FBS for 24 h until their evaluation [52]. The cells were treated for 24 h with metformin (25–150 μM) (European Pharmacopoeia, Sigma–Aldrich, St. Louis, MO, USA). Stock solution of metformin (M0605000, European Pharmacopoeia, Sigma–Aldrich, St. Louis, MO, USA) was prepared at a concentration of 6 mM in dimethyl sulfoxide (DMSO) (Panreac, Barcelona, Spain). The metformin concentration used for cell treatments were obtained by dilution of the stock solution in DMEM with 10% (v/v) FBS [45,53]. The final concentration of DMSO was always lower than 0.5% (v/v). α-tocopherol (Sigma–Aldrich, St. Louis, MO, USA) was prepared at a concentration of 10 mM in DMEM with 10% FBS and it was administrated at the same time as metformin to the cells and 24 h later, the cultures were exposed to PDT. Combined treatment was carried out when the cells reached 50–60% confluence. First, cells were incubated for 24 h with metformin (25–150 μM). Afterwards, metformin medium was replaced by MAL without FBS (0.3 mM, 5 h). Subsequently, cells were irradiated with red light source and the medium with MAL was replaced by fresh DMEM with 10% FBS and incubated for 24 h until evaluation [45,47]. The spheroids were treated under the same conditions as the 2D cells, on day 5 of their seeding.

2.4. Cellular viability and treatment combination analysis

Cell viability in 2D model was determined using the MTT (3-[4,5-dimethylthiazol-2-yl]-2,5-diphenyltetrazoliumbromide) assay (Sigma–Aldrich, St. Louis, MO, USA). MTT solution (100 μg/mL) was added to cell cultures and incubated at 37 °C for 3 h. After incubation, the formazan precipitate was dissolved with DMSO and optical density was measured in a SpectraFluor (Tecan, Bradenton, FL, USA) plate reader at 542 nm. Cellular toxicity was expressed as the percentage of surviving cells relative to that of the non-treated (control) cells. A statistical model based on cell survival percentage (CSP) was used to determine the magnitude of synergy observed after the combined treatment in both cell lines [54]. The model assumes that metformin and MAL-PDT have distinct mechanisms of action. $\mathrm{Dlog} = (\log \mathrm{CSP}_{\mathrm{metformin}} + \log \mathrm{CSP}_{\mathrm{PDT}}) - \log \mathrm{CSP}_{\mathrm{combination}}$. A Dlog > 2 indicates a synergistic effect, whereas an additive effect occurs when Dlog is 2. Cell survival in 3D models was analysed by the propidium iodide and acridine orange test. The spheroids were incubated with a PBS solution with a final concentration of both fluorochromes of 50 μg/mL. Immediately afterwards, the spheroids were observed in the fluorescence microscope under blue and green excitation light. The results were expressed as the percentage of green cells (all cells) with respect to red cells (dead) of the treated spheroids in relation to the control spheroids (not subjected to treatment) [55].

2.5. Array comparative genomic hybridization

For chromosomal array comparative genomic hybridization (CGH), DNA of SCC13 cells (P and 10GT) were isolated from exponential cultures using the Qiagen DNEasy Kit. Whole-genome analysis of the cells was conducted using a commercial 60-k oligonucleotide human array-CGH (AMADID 21924, Agilent Technologies, Santa Clara, CA, USA) following the manufacturer's protocol [56]. Healthy female DNA (Promega Biotech, Madison, WI, USA) was used as hybridization control. Microarray data were extracted and visualized using Feature Extraction software, v10.7 and Agilent Genomic Workbench, v5.0 (Agilent Technologies). Copy-number-altered regions were detected using ADM-2 (set as 6) statistic provided by DNA Analytics, with a minimum number of five consecutive probes. Microarray raw data tables have been deposited in the Gene Expression Omnibus under the accession number GSE180325. For the subsequent data treatment of the array, different databases were used such as NCBI, Reactome and Uniprot.

2.6. Cellular respiration determination and glycolysis rates

Cells were cultured in an XF 24-well cell culture microplate (Agilent technologies, Santa Clara, CA, USA) at a density of 30×10^3 cells/well in 200 μL of growth medium for 24 h. Then, 700 μL of XF Base Medium (Agilent technologies) supplemented with 25 mM glucose (Sigma–Aldrich, St. Louis, MO, USA), 1 mM pyruvate (Sigma–Aldrich), and 2 mM glutamine (Life Technologies, Carlsbad, CA, USA) were added, and the plate was incubated for 1 h at 37 °C without CO2. The final concentration and order of injected substances was 6 μM oligomycin (inhibits ATP synthase), 0.75 mM 2,4-Dinitrophenol (DNP) (an uncoupling agent that collapse the proton gradient and disrupts the mitochondrial membrane potential), 1 μM rotenone (inhibits complex I of the electron transport chain) plus 1 μM antimycin (inhibits complex III of the electron transport chain) (all from Sigma–Aldrich, St. Louis, MO, USA). To determine the rates of glycolysis, the initial amounts of lactate production were determined by the enzymatic quantification of lactate concentrations in the culture medium. Culture medium was replaced by fresh medium supplemented with 1% FBS 1 h before the measurement; 200 μL of culture medium samples were taken at different intervals (60 and 120 min) and precipitated with 800 μL of cold perchloric acid, incubated on ice for 1 h, and then centrifuged for 5 min at 11,000×g at 4 °C to obtain a protein-free supernatant. Supernatants were neutralized with 20% (w/v) KOH and centrifuged at 11,000×g and 4 °C for 5 min to sediment the KClO4 salt. Lactate levels were determined spectrophotometrically by following the reduction of NAD+ at 340 nm after the addition of 10 μL of lactate dehydrogenase (Sigma–Aldrich, St. Louis, MO, USA) [47].

2.7. Western blots

Western blotting was performed as previously described according to the standard protocol [47,57]. The primary antibodies used for western blotting were: pAMPK, (Thr172), AMPK, pAKT (ser473), AKT, phosho-p70S6K (Thr 389) and p70S6K (Cell Signaling Tecnology, Inc, Danvers, MA, USA), GAPDH, PKM2, α-tubulin (Abcam, Cambridge, UK), and β-F1-ATPase (clone 17/9–15G1) (Dr. Cuezva). Afterwards, membranes were subjected to the peroxidase–conjugated secondary antibody and developed by chemiluminescence (ECL, Amersham Pharmacia Biotech, Little Chalfont, UK) using the high-definition system ChemiDoc XRS+ (Bio-Rad, Hercules, CA, USA). The bands corresponding to the proteins were digitalized using the Image Lab, version 3.0.1 (Bio-Rad).

2.8. RNA extraction and RT-PCR

Total RNA was extracted and purified with the RNAeasy Mini Kit (Qiagen, Hilden, Germany). RNA concentration and purity was determined by spectrophotometry (NanoDrop ND1000, Nanodrop Technologies). The reverse transcription reactions were carried out from 1200 ng of total RNA from each sample using the High Capacity Reverse Transcription Kit (Applied Biosystems). The temperature conditions used were: a first step of 10 min at 25 °C, followed by 120 min at 37 °C and finally 5 s at 85 °C. mRNA expression was measured with TaqMan® probes (Supplemental Table 2) obtained from TaqMan® 96-well gene expression assay plates (Applied Biosystems, Thermo Fisher Scientific Inc, Rockford, IL, USA). Three

triplicates were performed for each sample and gene. The RT-PCR assay was carried out on the QuantStudio 7 Flex equipment (Applied Biosystems) in 384-well plates, starting from 5 ng of cDNA per well in a final volume of 10 μL containing the TaqMan® universal master mix II (Applied Biosystems). The protocol consisted of an initial denaturation cycle (10 min, 95 °C) and 40 amplification cycles (15 s, 95 °C; 1 min, 60 °C). The semi-quantitative analysis of the PCR results was performed using the DDCt method (LC480 1.5 software) that corrects the Cq data obtained with each sample for the analysed gene in relation to the value of the 18S ribosomal RNA reference gene. These analysis were carried out at the Genomics Unit of the Alberto Sols Biomedical Research Institute.

2.9. Cell cycle

Cell distribution throughout the cell cycle phases was studied by flow cytometry (Cytomics FC500, 2 laser, Beckman Coulter, Corston, UK). 24 h after metformin treatments, cells were trypsinized, fixed in 70% ethanol, and washed with PBS (phosphate buffered saline) by centrifugation. The pellet was resuspended in 50 μL of DNAprep kit (Beckman Coulter, Pasadena, CA, USA) and in 1 mL of propidium iodide and incubated for 30 min at 37 °C.

2.10. Protoporphyrin and reactive oxygen species production

Protporphyrin IX (PpIX) and reactive oxygen species (ROS) generation was evaluated by flow cytometry after treatments. For ROS evaluation, the cells were incubated with 6 μM of diacetate 2′-7′-dichlorodihydrofluorescein (DHF-DA) (Abcam, Cambridge, UK) for 1 h before the end of each treatment. Afterwards, cells were trypsinized, centrifuged 7 min at 1800 rpm, fixed with 1% formaldehyde in PBS at room temperature for 10 min and kept in the dark at 4 °C until evaluation. PpIX and ROS measurements were obtained using the flow cytometer FC500 Cytomics with a λexcitation of 625 nm and 490 nm, respectively, and a λemission of 670 nm and 530 nm, respectively. Fluorescence intensity was determined for 10^4 cells per condition.

2.11. Animal experiments

Xenograft mouse experiments were carried out in compliance with the guidelines in RD53/2013 (Spain) and was approved by the Ethics Committee from Consejo Superior de Investigaciones Científicas (CSIC, Madrid, Spain) and Comunidad Autónoma of Madrid (CAM, Consejería de Medio Ambiente; Register number: ES80790000188) in the frame of the projects FIS-PI15/00974 and FIS-PI18/00708 supported by the Spanish Ministerio de Economía y Competitividad. Female 6 weeks old athymic nude-Foxn1nu mice (Envigo, France) were used. Mice were classified randomly in two groups with 12 mice per group. One group was inoculated in both flanks with 2×10^6 SCC13 P cells in 50 μL of PBS and 50 μL of Matrigel (Corning, Bedford, MA, USA), and the other group was inoculated in both flanks with 1×10^6 SCC13 10GT cells [57]. In each group, mice were randomly distributed into two subgroups (6 mice per subgroup) and treated or not with 200 μg/mL metformin diluted in drinking water (PHR1084, Sigma—Aldrich, St. Louis, MO, USA) (Supplemental Table 3). Metformin was administered from day 7, when all tumors measured 35 mm^3, until the end of the experiment (28 days). The left tumor of each mouse was treated with PDT at day 11 after cell inoculation, when the tumors had reached a volume of 45 mm^3. For PDT, 2 mM MAL was administered by intratumoral injection in PBS. The volume of MAL administrated was equal to 50% of the volume of each tumor. After 4 h of dark incubation, tumors were exposed to 25 J/cm^2 of red light. During the subsequent days, the animals were monitored measuring the progressive increase of tumor size with an automatic caliper. To calculate the tumor volume, all the lobules formed from each inoculation were considered and determined as follows: $V = \Pi/6$ X (length X width X depth).

2.12. Hematoxylin and eosin stain (H & E); TdT-mediated dUTP nick-end labeling (TUNEL) assay; and immunohistochemistry analysis

Tissue sections were deparaffinized and dehydrated and H&E and TUNEL assays were performed as previously described according to the standard protocol [47]. For immunohistochemistry (IHC), endogenous peroxidase was inhibited with 3% hydrogen peroxide (Panreac, Barcelona, Spain) in methanol. The antigen unmasking was performed by immersing them in citrate buffer at pH 6 (0.25% citric acid and 0.038% sodium citrate in water) for 10 min in a pressure cooker. When the samples had tempered, blocking was carried out with non-immune serum (Dako, Agilent Technologies, Santa Clara, CA, USA) for 1 h at room temperature, followed by overnight incubation at 4 °C with the primary antibody (Ki67, GAPDH, PKM2 (Abcam, Cambridge, UK) and β-F1 -ATPase (Dr.Cuezva). After, the sections were incubated with the secondary antibody conjugated to streptavidin-peroxidase (Cell Signaling Tecnology, Inc, Danvers, MA, USA) for 30 min at room temperature. Color was developed by 3-amino-9-ethylcarbazole solution as chromogen (DAB, Vector laboratories, Burlingame, CA, USA) and hematoxylin counterstaining were performed following the manufacturer's protocol. Finally, the sections were dehydrated in increasing series of alcohol and mounted with DePeX (Serva, Heidelberg, Germany). Evaluation of IHC staining was performed by counting the number of cells with a grid that expressed the antigen studied, in 10 high-magnification representative fields. The percentage of positive cells was established for Ki67 using Cell Counter of Image J (NIH) whereas a semiquantitative method was used for β-F1—ATPase, GAPDH using IHC toolbox of Image J.

2.13. Statistical analysis

Data were expressed as the mean value of at least three experiments ± standard deviations (SD). The statistical analysis was carried out with the version 6.05 of the program GraphPad Prism (GraphPad Software Inc, USA) used, also, to make graphical representations. The statistical differences were determined using in general, analysis of variance (ANOVA, Chicago, IL, USA) and post hoc Bonferroni's test ($p < 0.05$). For tumor volume, nonparametric Kruskall—Wallis test was used and $p < 0.05$ was considered statistically significant. The significant differences were classified as *: $p < 0.05$; **: $p < 0.01$; ***: $p < 0.001$.

3. RESULTS

To investigate the resistance to PDT in sSCC we used two human cell lines (SCC13 and A431). These cells, called parental (P), were subjected to 10 PDT cycles to obtain the resistant 10G cells that were then inoculated in immunosuppressed mice. The induced tumors were subcultured by explants, and the new cell population was called 10GT, considering the fact that the *in vivo* microenvironment could promote the selection of cells with higher tumorigenic properties [47,50,57] (Fig. S1). After the generation of 10GT populations of sSCC cells (SCC13 and A431), their resistance to PDT was validated, in terms of cell survival, by the MTT assay by using 0.3 mM of MAL (5 h of incubation) and different light doses (0—30 J/cm^2). We decided to use this MAL concentration because differences in the response after PDT between P, 10G and 10GT cells were clearly observed (Fig. S2A). Furthermore, this concentration (0.3 mM) was the only one that allowed us to obtain a LD20 (lethal dose of 20%) in both P cells among

all the MAL doses used (0.1—1 mM) (Fig. S2B). In fact, the obtained data confirmed, as expected, that 10GT population of SCC13 and A431 cell were more resistant to PDT than their respective P and 10G cells (Fig. S2A). For all the experiments, the corresponding controls were performed: untreated cells (cells without MAL or light irradiation) and cells treated with MAL (0.3 mM, 5 h of incubation) or the highest red light used alone (30 J/cm^2). Under such treatment conditions, no cell toxicity was detected. According to these results, we selected the 10 GT population as resistant cells to PDT to perform the rest of the experiments. In addition, to evaluate the synergic effect with metformin, conditions of MAL-PDT that induced in the P populations a LD20 were selected (0.3 mM MAL and 23 J/cm^2 for SCC13 and 7 J/cm^2 for A431 cells).

3.1. Metabolic reprogramming involved in PDT resistant

As the resistance to treatment is significantly correlated with the accumulation of genomic alterations, we next performed an array CGH (Comparative Genomic hybridations) between both populations (P and 10GT) of the SCC13 cell line. We focused our attention on alterations at the level of energetic metabolism. Table 1 shows the percentage of altered genes of the main metabolic pathways for each cell population. The 10GT population presented between 10% and 20% altered genes compared to P population, which suggests that resistance to PDT implies modifications in cell metabolism genes. The alterations observed exclusively in the 10GT population related to these pathways were located on chromosomes 5, 11 and 19. In these chromosomes, the deletions were more frequent than duplications (Fig. S3). The main genes located in the chromosomal regions related to the indicated pathways are shown in Supplemental Table 4. In summary, in these deleted regions only one gene of glycolysis was observed: hexokinase 3 but several genes related to pyruvate metabolism were in these chromosomic regions, highlighting lactate dehydrogenase A and pyruvate dehydrogenase. Finally, a high number of genes encoding electron transport chain complexes, as well as those related to ATP formation, were also located in deleted regions, suggesting an OXPHOS dysregulation in PDT resistant cells.

Subsequently, we proceeded to validate the metabolic dysregulation observed in the array CGH. To do this, we performed an analysis of OXPHOS and glycolysis in P and 10GT populations of both cell lines (SCC13 and A431) (Figure 1). In order to determine OXPHOS, we analysed the oxygen consumption rate. The results obtained indicated that 10GT populations (of both cell lines) displayed lower OCR than their corresponding P populations (Figure 1A—B). In addition, we also determined the oligomycin sensitive respiration rate (OSR), which represents the activity of synthesis of ATP by complex V coupled to the respiratory chain. As expected, the resistant cells of both cell lines showed a significant decrease in OSR, suggesting a lower synthesis of ATP (Figure 1C). Finally, we also evaluated the expression of the β-F1-ATPase/GAPDH ratio, a proteomic index of the overall mitochondrial metabolism of the cell, at the protein level by western blot (WB). This ratio was significantly decreased in both 10GT populations, suggesting a lower OXPHOS in these cells compared to their corresponding P cells (Figure 1D). All these results support the ones obtained from the array CGH analysis, indicating that the generation of PDT resistant cells triggers a dysregulation of OXPHOS.

On the other hand, we analysed the glycolytic state of the PDT resistant cells. Glycolytic flux was evaluated by measuring extracellular lactate production. We did not observe significant differences between P and 10GT populations of SCC13 cells. However, the 10GT population of A431 showed a higher lactate production than that of P population, according to the OXPHOS diminution observed (Figure 1E). Finally, we analysed the expression of PKM2, which is an isoform of pyruvate kinase that promotes aerobic glycolysis. Consistently, the PKM2 levels were significantly increased in both PDT resistant cells (Figure 1F).

Table 1 — Percentage of altered genes in pathways related to energy metabolism. We analysed it by the reactome online platform from the results of the array CGH.

Pathways	Modified genes (%)	
	P SCC13	10 GT SCC13
Glycolysis	2.7	7.3
Pyruvate metabolism	8.8	21.0
Krebs cycle	12.0	20.0
Electron transport chain	15.6	36.5
ATP production	8.6	17.3

3.2. Metformin as adjuvant to PDT *in vitro*

Previous results indicated that 10GT cells had decreased mitochondrial metabolism and showed a partial increase of glycolysis. Therefore, we proceeded to evaluate the effect of metformin as a potential treatment against sSCC cells resistant to PDT. The P and 10GT cells were pre-incubated 24 h with metformin (25—150 μM) and subsequently PDT treatment were administrated (0.3 mM MAL, 5 h, and 23 J/cm^2 in SCC13 cell line and 7 J/cm^2 in A431 cell lines). We observed a significant decrease in cell survival after the combined treatment in both populations of SCC13 and A431. These results agree with the cell morphology after combined treatment, which showed cytoplasmic retraction with a rounded aspect similar to that of cells in apoptosis (Figure 2A). This decrease was dependent on the metformin concentration, being greater with the higher concentrations. In addition, the type of effect (synergistic, additive or antagonistic) produced by the combination of treatments was analysed by estimating the Dlog value (calculated as indicated in the Materials and Methods section). In both sSCC cell lines Dlog values were greater than 2 from 75 μM metformin, confirming the synergistic effect of MAL-PDT and metformin (Figure 2B). For this reason, the 75 μM dose was selected for the rest of experiments.

After the excellent results obtained in monolayer cultures by the combination of metformin and PDT, we then proceeded to assess their efficacy in three-dimensional models (spheroids). On the fifth day after spheroids seed, they were treated with metformin (75 μM, 24 h) and then PDT was administrated (0.3 mM MAL, 5 h, and 23 J/cm^2 in SCC13 cell line and 7 J/cm^2 in A431 cell lines). The survival of the cells confirming the spheroids was assessed, 24 h after irradiation, by staining with propidium iodide-acridine orange (Figure 2C). The results obtained showed that both untreated spheroids (control) and metformin treated presented a green fluorescence, indicating that all the cells that comprise them were alive. PDT treatments showed some red fluorescence in P spheroids, indicating cell death. Finally, the application of the combined treatment caused an increase in red fluorescence, suggesting a significant decrease in the survival of the cells that form the spheroids. Therefore, the combination of both treatments has a greater cytotoxic effect on 3D cultures than metformin or PDT treatments administered individually (Figure 2C).

3.3. Metformin as adjuvant to PDT *in vivo*

Considering the obtained *in vitro* results, we selected the SCC13 cell line to perform tumor studies since these cells showed better response to PDT. P and 10GT SCC13 cells were inoculated in nude mice to induce tumors in order to evaluate the potential antitumor activity of the combined treatment: metformin plus PDT. Figure 3A shows the data

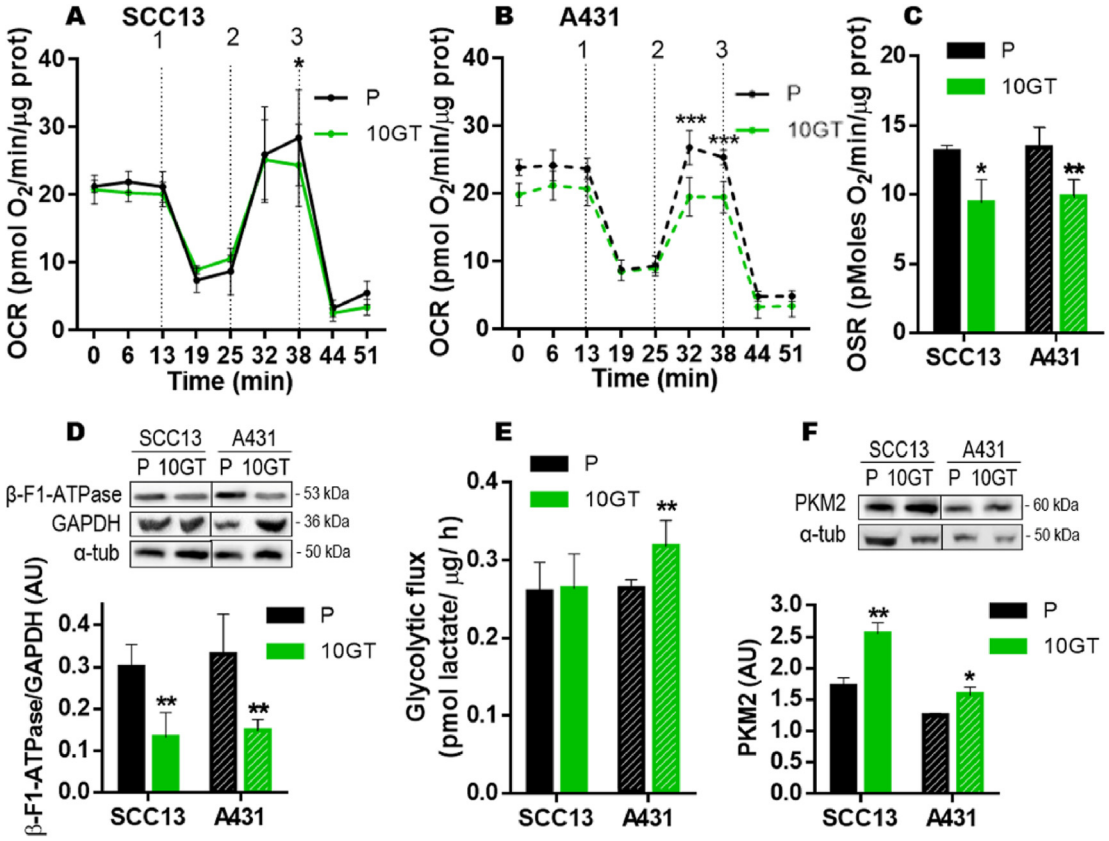

Figure 1: Metabolic characterization of sSCC. (A) Oxygen consumption rate (OCR) in SCC13 cells, measurements over time (min), were determined by using an extracellular flux analyser after the sequential addition of oligomycin (1), 2,4-Dinitrophenol (DNP) (2), and rotenone + antimycin (3). **(B)** Oxygen consumption rate (OCR) in A431cells. **(C)** Oligomycin-sensitive respiration, which represents the activity of oxidative phosphorylation (OXPHOS), was calculated as basal respiration − oligomycin respiration. **(D)** Expression of the metabolic markers β-F1-ATPase and GAPDH (glyceraldehyde-3-phosphate dehydrogenase) analysed by WB; α-tubulin was used as loading control; and the ratio of β-F1-ATPase/GAPDH indicates the use of glucose by the cells. **(E)** Rates of lactate production determined spectrophotometrically. **(F)** Pyruvate kinase M2 (PKM2) levels, analysed by WB; α-tubulin was used as loading control. Values were represented as mean ± SD (*: $p< 0.05$; **: $p< 0.01$; ***: $p< 0.001$) ($n = 4$).

obtained regarding the evolution of the tumors volume throughout the experiment. Tumor photographs and tumor weight at the end of the experiment (day 28) are shown in Fig. S4. The tumors generated by P population responded better to the treatments (metformin, PDT and combined) than those formed by the 10GT populations. The three treatments in P showed a decrease in their size compared to untreated controls. The combined treatment was the one that presented the greatest reduction in tumor size, being significant compared to the other conditions. In the case of tumors generated by 10GT populations, a significant decrease in their size was observed after combined treatment (metformin + PDT) (Figure 3A). The histological characteristics of these tumors were evaluated by H&E staining and showed the presence of nuclear pleomorphism and muscle infiltration. The treatments (metformin, PDT and combined) did not cause significant changes at the level of tumor morphology. However, areas of extravasation of red blood cells were observed after them, being more striking after the combined treatment application (Figure 3B). The results obtained by TUNEL assay showed a correlation with the histopathological studies; numerous dead cells were observed close to the extravasation sites. PDT produced a significant increase in TUNEL-positive cells in all tumors, being greater in those generated by P populations, with respect to the resistant ones. Finally, the combined treatment (metformin and PDT) caused a greater significant increase in dead cells compared to the individualized treatments (Figure 3C).

3.4. Metformin modulates metabolic reprogramming. Prognostic markers

The above results showed that metformin treatments sensitized the 10GT populations to PDT in both cell lines (SCC13 and A431), which presented a lower OXPHOS metabolism than their P. Therefore, we next evaluated the metabolism of these cells after metformin treatment (75 µM, 24 h). The OCR after metformin treatment showed a significant increase in the maxima respiration (after addition of DNP (2)) in 10GT population of SCC13 cells (Figure 4A) and in both populations of A431 (Figure 4B), suggesting an intensification of OXPHOS. These results were in concordance with that obtained in OSR after metformin treatment, where both resistant cells showed a significant increase (Figure 4C). Finally, all the cell lines showed a significant diminution in the lactate extracellular production, suggesting a reduction of the glycolytic flux after metformin treatment (Figure 4D). The set of results obtained hints at the PDT resistant cells of sSCC increase their OXPHOS and reduce their glycolytic flux after metformin, suggesting that metformin modulates metabolic reprogramming in these cells.

On the other hand, one of the main effects of metformin is the arrest of the cell cycle. Therefore, we evaluated that our metformin doses stopped the cell cycle *in vitro* (75 µM, 24 h) and *in vivo* (200 µg/mL diluted in drinking water) in both populations (Figure 5A—B, Fig. S5A). *In vitro*, we observed that P and 10GT populations of both sSCC cell lines (SCC13 and A431) showed a significant arrest in G0/G1

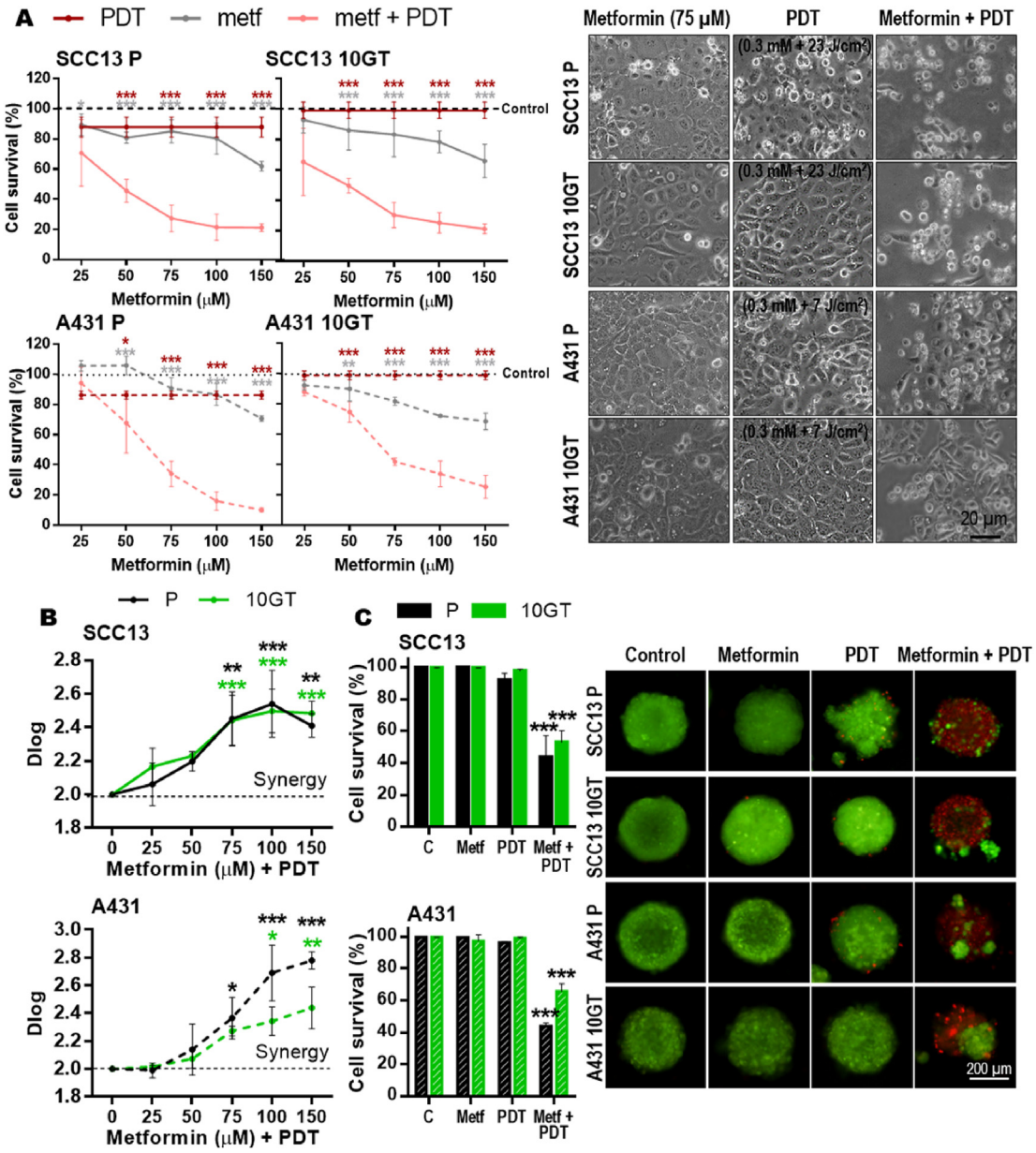

Figure 2: Combined treatment of metformin and PDT in sSCC cells. **(A)** Cells were treated for 24 h with metformin (25—150 μM) and then subjected to PDT (0.3 mM MAL and 23 J/cm^2 in SCC13 and 7 J/cm^2 in A431 cells). The results were evaluated 24 h after treatment by MTT test. A representative image of the effect of the treatments on the different cell lines is shown by phase contrast microscopy. **(B)** Combined treatment provided a synergistic effect on cell viability in both populations of SCC13 and A431 cells. The synergy/antagonism parameter Dlog (difference in logarithm) was calculated as calculated as indicated in the Materials and Methods section. **(C)** Evaluation of the combined treatment in spheroids (3D model). The spheroids were grown for 4 days before being treated for 24 h with metformin (75 μM), subsequently they were treated with PDT (0.3 mM MAL and 23 J/cm^2 in SCC13 and 7 J/cm^2 in A431 cells). Cell survival was evaluated by staining the spheroids with propidium iodide-acridine orange. The quantification of cell survival was determined by the percentage of green cells to red cells. Values were represented as mean ± SD (*: $p< 0.05$; **: $p< 0.01$; ***: $p< 0.001$) ($n = 5$). Metf: metformin.

associated with a decrease in S and G2 phase (Figure 5A). To be sure that metformin alone does not induce cell death, the subG population after the treatment is shown in Fig. S5B. However, in SCC13 tumors only P tumor showed a decreased of Ki67 (proliferation markers) after metformin treatment (Figure 5B). Likewise, we evaluated the bioenergetic index (β-F1-ATPase/GAPDH) and PKM2 expression as possible prognosis markers of response to PDT. In both cell lines and SCC13 tumors, we observed a higher bioenergetic index that was associated with a better response to PDT. After metformin treatment, the values of this marker increased, except in 10GT tumors that they did not show a better response after the combined treatment (Figure 5C—D). However, metformin did not induce significant difference in PKM2 expression neither *in vitro* nor *in vivo*, even though the 10GT populations showed the highest levels (Figure 5E—F).

3.5. Metformin enhances PDT mechanism of action

Since the combined treatment improved the response to PDT, we evaluated if metformin treatment by itself increased the PpIX intracellular production, since this metabolite is the basis of PDT action. PpIX production was determined by flow cytometry in P and 10GT

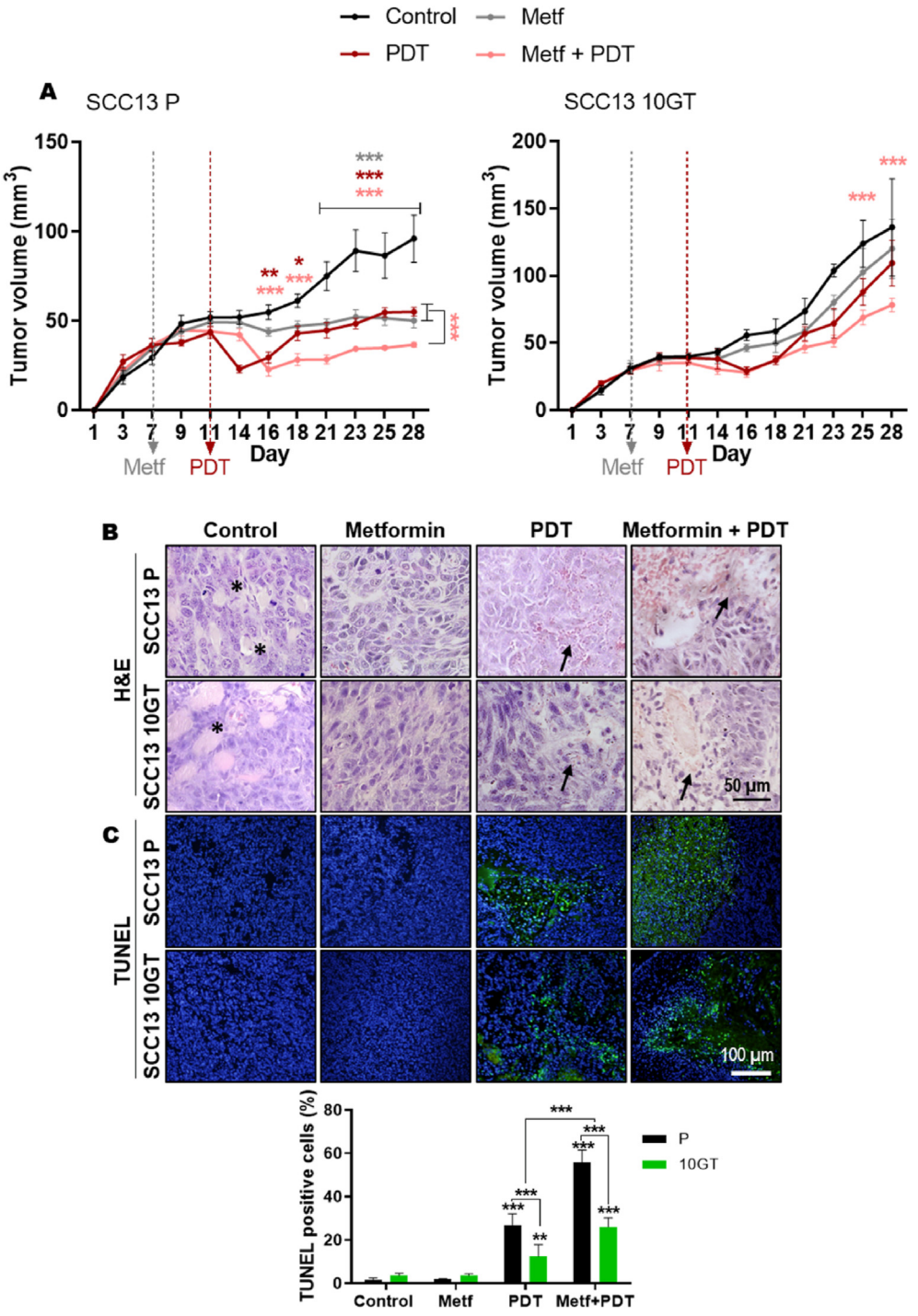

Figure 3: Combined treatment of metformin and PDT in SCC13 tumors induced in mice. **(A)** Tumor volumes evolution over time after the treatments in P and 10GT SCC13 tumors. At day 7, tumors were treated with metformin (200 µg/mL diluted in drinking water along the rest of the experiment). At day 11 the tumors were subjected to PDT (2 mM MAL, 4 h of incubation, and 25 J/cm^2 of red light). Scale bar = 10 mm. **(B)** Tumor sections at the end of the experiments stained with hematoxylin and eosin (H&E) and **(C)** TUNEL assay (dead cells appeared fluorescing in green and nuclei fluorescing in blue). Values were represented as mean ± SD (*: $p < 0.05$; **: $p < 0.01$; ***: $p < 0.001$) (n = 3).

populations of both sSCC cells prior incubation with MAL (basal level PpIX), after metformin (75 µM, 24h), MAL (0.3 mM, 5h), and after metformin treatment followed by MAL (Figure 6A). Cells treated with metformin did not show any differences in PpIX production respect to untreated control cells. MAL incubation only induced a significant increase in P population of A431 cells respect to untreated cells, however if we use a higher MAL concentration (0.5 mM) we observed a significant increase in the PpIX production (Fig. S6A). Finally, the combined treatment (metformin + MAL) in both populations (P and 10GT) of sSCC cells induced significant differences in PpIX production with respect to the rest of the conditions (Figure 6A). Likewise, we evaluated the ROS generation, as the main cause of cell death after

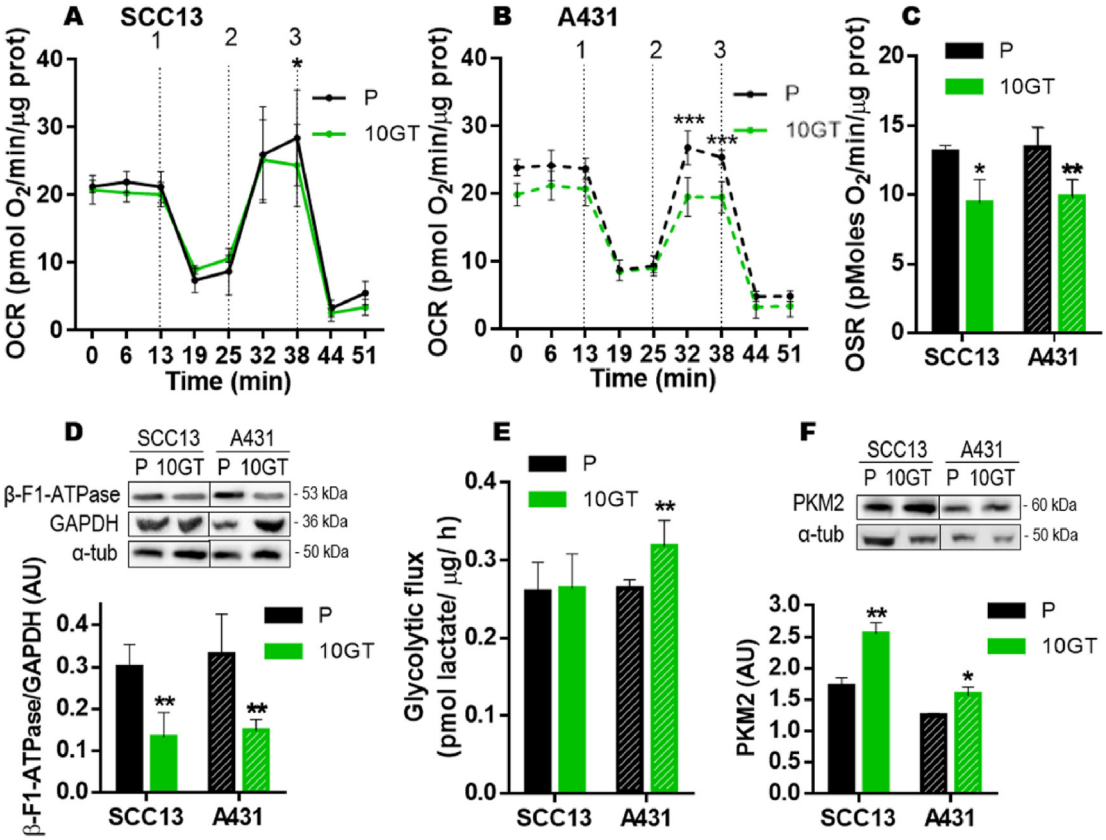

Figure 4: Metformin treatment (75 µM, 24h) in sSCC cells. (A–B) Real-time analysis of OCR in **(A)** SCC13 and **(B)** A431 cells were determined by using an extracellular flux analyser after the sequential addition of oligomycin (1), 2,4-Dinitrophenol (DNP) (2), and rotenone + antimycin (3). **(C)** Oligomycin-sensitive respiration, which represents the activity of oxidative phosphorylation (OXPHOS), was calculated as basal respiration − oligomycin respiration. **(D)** Rates of lactate production determined spectrophotometrically. Values were represented as mean ± SD (*: $p< 0.05$; **: $p< 0.01$; ***: $p< 0.001$) ($n = 4$).

PDT. ROS levels were also assessed by flow cytometry. The results obtained showed a significant increase in ROS levels after the combined treatment (metformin −24 h, 75 µM- + PDT -5 h, 0.3 mM MAL following red light 23 J/cm^2 in SCC13 and 7 J/cm^2 in A431-), in accordance with the lower percentage of cell survival observed after this treatment and α-tocopherol treatment, a known antioxidant, significantly reduced the cell death induced by PDT (Figure 6B, S6A-B).

3.6. mTOR pathway modulation by combined treatment

One of the main pathways related to tumor processes and glycolytic phenotype induction is PI3K/AKT/mTOR pathway. In this sense, and in a first approach, we proceeded to analyse the mRNA levels of participants in this signaling pathway by RT-PCR in both populations of SCC13 cell line. The results at the mRNA level showed a significant increase in the 10GT population of *PIK3CA* (alpha catalytic subunit of PI3K), *AKT1*, *mTOR*, *S6KB1* (p70S6K, ribosomal protein S6 kinase β1), *PDK1* (phosphoinositide dependent kinase 1) and *SLC2A1* (GLUT1) compared to its P population. All these genes are related to an increased glycolytic activity (Fig. S7). Next, we evaluated the impact of the different treatments on their expression (Figure 7A–F). The results showed a tendency to decrease the levels of these mRNAs (*PIK3CA* (Figure 7A), *AKT1* (Figure 7B), *mTOR* (Figure 7C), *S6KB1* (Figure 7D), *PDK1* (Figure 7E) and *SLC2A1* (Figure 7F)) after all treatments (metformin, PDT and combined) in the 10GT population. After the combined treatment, the reduction of expression levels was greater in *AKT1*, *mTOR* and *S6KB1*. These results suggest that the combination of treatments favors the inhibition of this signaling pathway. Finally, we analysed mRNA levels both AMPK α catalytic subunits (*PRKAA1*, *PRKAA2*), which have been reported that can inhibit mTOR pathway by metformin treatment. The results showed that the expression of *PRKAA1* increased after the three treatments in the P population and after the combined one in the 10GT population (Figure 7G). In addition, the expression of the *PRKAA2* increased in both populations after treatment with metformin and combined, being significant after the latter (Figure 7H). In summary, the results obtained indicated that in both populations of SCC13 the treatments, especially the combination of metformin and PDT, reduced the levels of *AKT1*, *mTOR* and *S6KB1* mRNA; this inhibition could be dependent on AMPK. Therefore, these results were then confirmed at the level of protein expression using WB in both populations of sSCC cell lines (SCC13 and A431) (Figure 7I).

4. DISCUSSION

PDT has a relapse rate of up to 30% 5 years after the treatment in sSCC. The main objective of this study was to determine the role played by metabolic reprogramming in the resistance process to MAL PDT in sSCC. For this, we have used the human SCC cell lines: SCC13 [48] and A431 [49], which we have been called parental (P) and their PDT-resistant cells (10GT) [57]. Even clinical PDT cases involve one or two cycles of MAL-PDT, in our work we have used a model based on repeated PDT in order to select highly resistant cells and with a stable

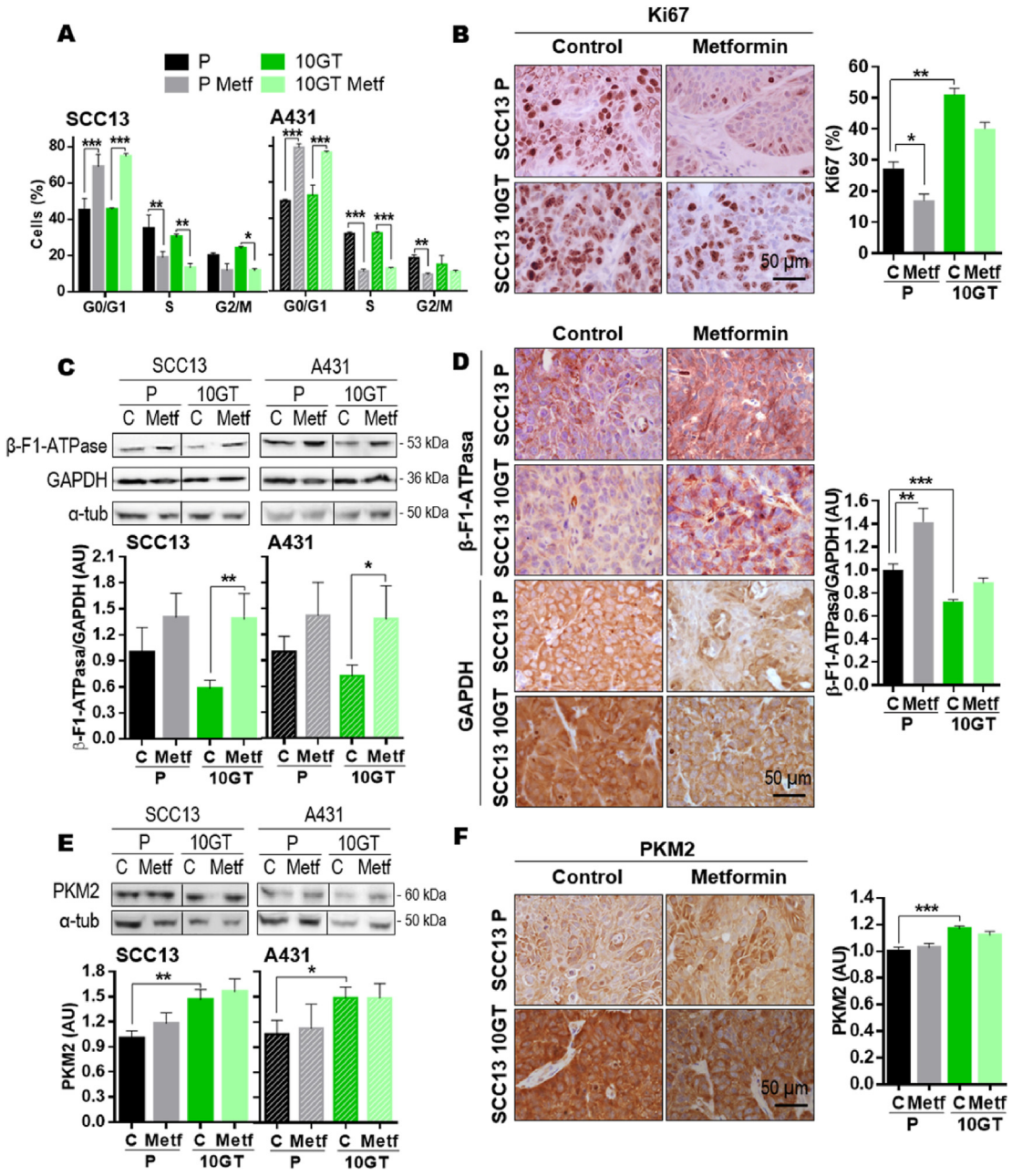

Figure 5: Metformin treatment in vitro and in vivo sSCC. (A) Effect metformin treatment (75 μM, 24 h) on cell cycle progression in P and 10GT populations of SCC13 and A431 cells. Cell cycle distribution was analysed by flow cytometry. **(B)** Ki67 expression in control and metformin treatment in P and 10GT SCC13 tumors evaluated by IHC. **(C)** Bioenergetic index analysed by WB after metformin treatment in SCC13 and A431 cells; α-tubulin was used as loading control. **(D)** Bioenergetic index evaluated by IHC in control and metformin treatment in P and 10GT SCC13 tumors. **(E)** PKM2 expression analysed by WB after metformin treatment in SCC13 and A431 cells; α-tubulin was used as loading control. **(F)** PKM2 expression evaluated by IHC in control and metformin treatment in P and 10GT SCC13 tumors. Values were represented as mean ± SD (*: $p < 0.05$; **: $p < 0.01$; ***: $p < 0.001$) ($n = 3$).

resistance phenotype [41,50,57]. By using this model, the present study shows that the generation of sSCC cells resistant to PDT implies a process of metabolic reprogramming towards aerobic glycolysis, which favors resistance to treatment. Although, this resistance in sSCC, maybe is not involved in PDT mediated by other exogenous photosensitizers, since it was generated by the MAL compound. Likewise, metformin, a drug used clinically for the treatment of type II diabetes, is capable of modulating the glycolytic metabolism and sensitize PDT resistant cells, both *in vitro* and *in vivo*.

Glycolysis and OXPHOS are the main metabolic pathways of energy production in cells. The metabolic reprogramming that tumor cells undergo is related to a stimulation of aerobic glycolysis and partial inhibition of OXPHOS. This metabolic change was first described by Otto Warburg, being the basic principle underlying the PET- FDG (positron emission tomography using 18-fluorodeoxyglucose) diagnostic technique [25,58–61]. The array CGH performed in the SCC13 cell line, allowed us to relate the generation of PDT resistance with modifications in the chromosomal regions where the genes that

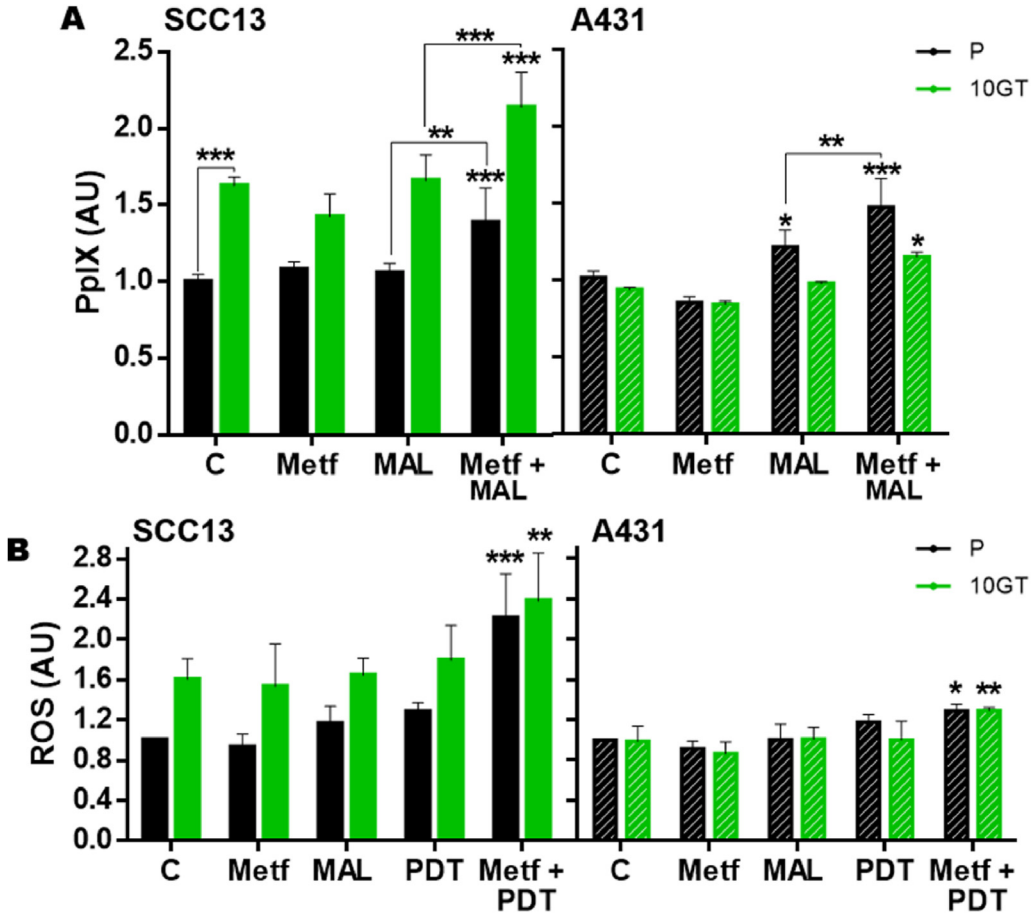

Figure 6: Combined treatment effect on sSCC cell lines relating to PDT pathway. **(A)** PpIX production was evaluated by flow cytometry after incubation with metformin (24 h, 75 μM), MAL (5 h, 0.3 mM), and metformin plus MAL (24 h followed by 5 h, respectively). **(B)** ROS generation was evaluated by flow cytometry after incubation with metformin (24 h, 75 μM), MAL (5 h, 0.3 mM), PDT (MAL following red light −23 J/cm^2 in SCC13 and 7 J/cm^2 in A431-) and combined treatment (metformin plus PDT).Values were represented as mean ± SD (*: $p < 0.05$; **: $p < 0.01$; ***: $p < 0.001$) ($n = 3$).

encode the electron transport chain complexes are found. These genetic differences were generated by PDT and amplified in xenograft (Supplemental Table 4). Some of these genes have been linked to mitochondrial dysfunction in other types of cancer, such as dysregulation of succinate dehydrogenase in ovarian cancer [62] and decreased expression of genes that encode the complex I (NDUFA2 and NDUFS7) and complex III (UQCR11, UQCRQ) in triple negative lung cancer [63]. OCR, OSR and bioenergetic index analysis were performed to corroborate the loss of OXPHOS in 10GT populations [36,37]. The bioenergetic index has been proposed as a prognostic marker in colon, breast, lung and melanoma carcinoma [39,64,65] and in skin cancer progression [66]. In this sense, our results support the value of this index as indicative of a worse response to PDT. On the other hand, at the glycolytic level, the expression of PKM2 *in vitro* and *in vivo* showed a significant increase in 10GT populations with respect to its P. PKM2 is an isoform of PK that is overexpressed in many types of tumors and is an important regulator of glycolytic activity. Its mechanism of action is not completely defined, although numerous articles relate its overexpression to an increase in glucose consumption and lactate production [34,67]. The expression of PKM2 increased is being used as a poor prognostic marker in other types of cancer, such as squamous cell carcinoma of the cervix [68], intrahepatic cholangiocarcinoma [69], squamous cell carcinoma of the esophagus, and breast cancer [70]. We could observed a correlation between glycolytic flux and PKM2 expression in A431 cell, indicating a reprogramming of metabolism towards aerobic glycolysis in its 10GT population. However, in 10GT population of SCC13 cell, which showed higher expression of PKM2, no changes in glycolytic flux were observed. This inconsistency could be explained from the results of the array CGH, since the responsible genes for the transformation of pyruvate into lactate were found in deleted chromosomal regions. Therefore, it is likely that pyruvate is transformed, instead of lactate, into oxaloacetate by the enzyme pyruvate carboxylase (found in a region with trisomy), forming intermediate metabolites used for tumor growth [71]. In summary, these results, the evidence of the increase in aerobic glycolysis and the decrease in OXPHOS and a worse response to the treatments, [28,29] allow us to conclude that metabolic reprogramming is a key factor in the lack of response to PDT in sSCC.

Given our findings related to metabolic reprogramming in PDT resistant cells and that one of the main advantages of this therapy is it easy application in combination with other therapies, we evaluated the efficacy of the combination of PDT with metformin. Metformin has been shown to have antitumor properties in combination with other treatments [44–47]. The results obtained showed that the pretreatment with metformin improved the efficacy of PDT in P and 10GT populations of both sSCC cell lines. The increased cytotoxicity was due to a

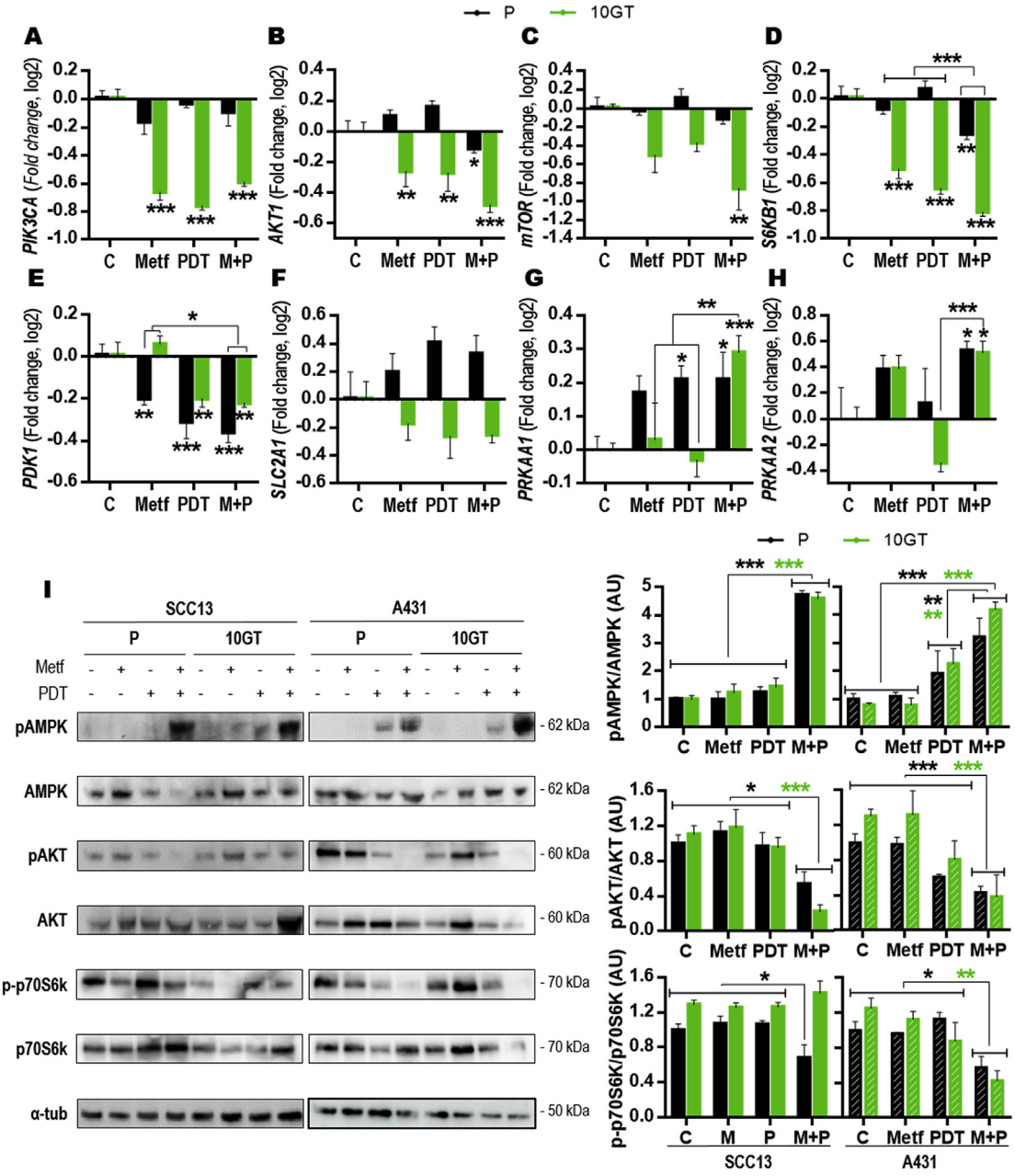

Figure 7: PI3K/AKT/mTOR pathway after combined treatment. N mRNA expression of **(A)** *PIK3CA*, **(B)** *AKT1*, **(C)** *mTOR*, **(D)** *S6KB1*, **(E)** *PDK1*, **(F)** *SLC2A1*, **(G)** *PRKAA1*, **(H)** *PRKAA2* in both populations (P and 10GT) of SCC13 cell line by RT-PCR after incubation with metformin (24 h, 75 μM), PDT (0.3 mM MAL following 23 J/cm^2 red light) and combined treatment (metformin plus PDT). **(I)** Expression by western blot of AMP-activated protein kinase (AMPK)-mammalian target of rapamycin (mTOR) pathway components: pAMPK, AMPK, pAKT, AKT, p-p70S6K and p-p70S6K after treatments (metformin, MAL-PDT, and metformin plus MAL-PDT). A representative experiment of each marker is shown, and pAMPK/AMPK, pAKT/AKT, and p-p70S6K/p70S6K densitometry graphics of both P and resistant populations of SCC13 and A431 cells are shown. A-tubulin was used as loading control. Values were represented as mean ± SD (*: $p< 0.05$; **: $p< 0.01$; ***: $p< 0.001$) ($n = 3$) M + P: metformin + PDT.

synergistic effect between both treatments, metformin and PDT. The efficacy of the combined treatment was also evaluated in a 3D model (spheroids). Compared to 2D models, spheroids can more accurately mimic some characteristics of solid tumors, such as their spatial architecture, gene expression patterns, physiological responses, and drug resistance mechanism [50,72,73]. Thus, at the 3D level, we were able to verify the greater efficacy of the combined treatment in all cell lines (SCC13 and A431) and in both cell populations (P and 10GT) compared to individualized treatments. Considering *in vitro* results, we perform studies in xenotransplanted tumors. In the tumors formed by P and 10GT populations, combined treatment significantly reduced the tumor volume. There are several studies that link the efficacy of combined metformin treatment together with chemotherapeutic drugs with an increase in cell death and a reduction in tumor size [74–76]. In our results, all tumors exposed to the combined treatment presented an increase in cell death. However, this increase in cell death was not accompanied by a significant reduction in tumor size in 10GT tumors. The antitumor function of metformin is also related to cell cycle arrest,

which leads to the stabilization of tumor growth [75,77,78]. Even so, we can conclude that metformin improves the efficacy of PDT, both *in vitro* and *in vivo,* in 10GT and P populations of sSCC.

Metformin has been reported to be effective as adjuvant in the treatment of different types of cancer by interfering with metabolic reprogramming mechanisms. Therefore, we proceeded to evaluate whether metformin could modulate the metabolic reprogramming observed in 10GT populations. In relation to OXPHOS (*in vitro* and *in vivo*), both populations of sSCC showed a significant increase in all evaluated OXPHOS markers (bioenergetic index, OCR and OSR). This result is not related to that observed in other tumor lines, in which an inhibition of OXPHOS has been described, although it is important to note that in all these studies the metformin concentrations used were higher than those used in our study [42,43,47]. Furthermore, a recent studies revealed that doses higher than 75 μM of metformin caused a decrease in OXPHOS, while lower concentrations increased it [79,80]. At glycolytic flux, both populations of sSCC reduced extracellular lactate production after metformin treatment, indicating a reduction in aerobic glycolysis. This decrease in glycolytic flux has been observed in cancer cells from cervix and hepatoma, in which metformin deregulates GLUT and inhibits key enzymes of aerobic glycolysis such as PK and LDH [81,82]. However, in colon and breast cancer, a decrease in glycolytic enzymes has not been documented [83], as in our results, PKM2 after metformin treatment was not modified, indicating that antidiabetic treatment appears to exert different effects on glycolysis depending on the type of cancer cells. In any case, metformin treatment modulated the metabolic reprogramming observed in PDT resistant of sSCC cells.

One of the main mechanisms of action of metformin is the inhibition of the AKT/mTOR pathway [42,43], which is also one of the critical points of positive control of the Warburg effect in tumor cells [32,75]. The activation of this pathway has been related to resistance to different chemotherapeutics in several carcinomas [84—88]. Likewise, the inhibition of participants of this pathway is being evaluated as chemosensitizers [89—92]. In this sense, the results obtained in the 10GT population of SCC13 cells revealed an increase in mRNA levels, compared to its P population, of PI3K (*PI3KCA*), *AKT1*, *mTOR*, p70S6K (*S6KB1*), *PDK1* and GLUT1 (*SLC2A1*), suggesting that these molecules could be responsible for the reprogramming towards aerobic glycolysis and, therefore, for its resistance to PDT. In this cell line, after combined treatment, the mRNA levels of *AKT*, *mTOR* and *S6KB1* were reduced and the levels of the catalytic AMPK α subunits (*PRKAA1*, *PRKAA2*) increased significantly, suggesting that the AKT/mTOR pathway inhibition and the AMPK activation would be related to the increase in the efficacy of the combined treatment. The results were validated at the AMPK, AKT and p70S6K protein expression by WB analysis in both sSCC cell lines. Other studies also associate the efficacy of the combination of metformin with chemotherapeutic agents with a suppression of the AKT/mTOR pathway through AMPK activation [75,93,94].

Finally, there are numerous studies that link the PpIX production and the ROS generation with a higher efficiency of PDT [13,16,18]. In our case, the selected PDT dose only induced a LD20 in P cells but allowed us to better observe the effect of the combined treatment. This could be the reason why we did not see a high increase in PpIX production and ROS generation after PDT alone. If we increased the MAL concentration we can detect the expected effect, a hight PpIX and ROS production (Fig. S6A). However, both populations of sSCC cells showed an increase in PpIX generation and intracellular ROS production after combined treatment, suggesting that metformin promotes the photo-reactivity to PDT and therefore increases its efficacy in sSCC cells.

5. CONCLUSIONS

Increased aerobic glycolysis and OXPHOS dysregulation promote resistance to MAL-PDT in sSCC, both *in vitro* in cell cultures and *in vivo* in induced tumors in mice. In addition, increased PKM2 expression and decreased bioenergetic signature (β-F1-ATPase/GAPDH ratio) are markers of poor response to PDT in sSCC. On the other hand, metformin treatment modulates the glycolytic metabolism and it increases OXPHOS in PDT resistant sSCC cells. Finally, the treatment with metformin prior to PDT (combined treatment) improved the cytotoxic effect on P and 10GT cells. The combined treatment is caused for an increase in protoporphyrin IX production, reactive oxygen species generation, AMPK expression and the inhibition of AKT/mTOR pathway. The greater efficacy of combined treatments is also seen *in vivo*, in induced tumors by SCC13 cells inoculation. Our results support the possible adjuvant role of metformin and place the combined treatment (metformin and PDT) as a potential therapy against sSCC.

FUNDING

This research was supported by Spanish grants from Instituto de Salud Carlos III MINECO and Feder Funds (FIS PI15/00974; PI18/00858 and PI18/00708) and Ministerio de Ciencia, Innovación y Universidades (PID2019-108674RB-100).

AUTHOR CONTRIBUTIONS

MM: Formal analysis; Investigation; Methodology; Writing — original draft; Writing - review and editing.
MG: Methodology; collaborated with *in vivo* experiments
JN: Methodology, collaborated with *in vitro* experiments
MP: Methodology, collaborated with *in vitro* experiments
JMC: Formal analysis; Writing - review and editing; Supervision; Funding acquisition
SG: Conceptualization; Formal analysis; Writing - review and editing; Supervision
YG: Conceptualization; Formal analysis; Writing - review and editing; Supervision; Funding acquisition
AJ: Conceptualization; Formal analysis; Writing - review and editing; Supervision; Funding acquisition

ACKNOWLEDGEMENTS

We wish to acknowledge Flow Cytometry service and animal facility from Centro Nacional de Biotecnología (Madrid, Spain). We also thank you to Genomics Core Facility at the Instituto de Investigaciones Biomédicas "Alberto Sols" (Madrid, Spain) and NIMGenetics (Madrid, Spain). Finally, we are grateful to Dr. Nuevo Tapioles for the help to carry out this work.

CONFLICT OF INTEREST

None declared.

APPENDIX A. SUPPLEMENTARY DATA

Supplementary data to this article can be found online at https://doi.org/10.1016/j.molmet.2022.101496.

REFERENCES

[1] Burton, K.A., Ashack, K.A., Khachemoune, A., 2016. Cutaneous squamous cell carcinoma: a review of high-risk and metastatic disease. American Journal of Clinical Dermatology 17:491–508. https://doi.org/10.1007/s40257-016-0207-3.

[2] Barton, V., Armeson, K., Hampras, S., Ferris, L.K., Visvanathan, K., Rollison, D., et al., 2017. Non-melanoma skin cancer and risk of all-cause and cancer-related mortality: a systematic review. Archives of Dermatology 309:243–251. https://doi.org/10.1007/s00403-017-1724-5.

[3] Diepgen, T., Mahler, V., 2002. The epidemiology of skin cancer. British Journal of Dermatology 146:1–6. https://doi.org/10.1046/j.1365-2133.146.s61.2.x.

[4] Rudolph, R., Zelac, D.E., 2004. Squamous cell carcinoma of the skin. Plastic and Reconstructive Surgery 114:82e–94e. https://doi.org/10.1097/01.PRS.0000138243.45735.8A.

[5] Kolk, A., Wolff, K.D., Smeets, R., Kesting, M., Hein, R., Eckert, A.W., 2014. Melanotic and non-melanotic malignancies of the face and external ear – a review of current treatment concepts and future options. Cancer Treatment Reviews 40:819–837. https://doi.org/10.1016/j.ctrv.2014.04.002.

[6] Racz, J., Joshua, A.M., Lipa, J.E., Sun, A., Wright, F.C., 2016. In: Wright, F., Escallon, J., Cukier, M., Tsang, M., Hameed, U. (Eds.), Non-melanoma skin cancer, 2nd ed. Toronto: Springer. Surgical Oncology Manual. p. 225–32.

[7] Madan, V., Lear, J.T., Szeimies, R.M., 2010. Non-melanoma skin cancer. The Lancet 375:673–685. https://doi.org/10.1016/S0140-6736(09)61196-X.

[8] Liu-Smith, F., Jia, J., Zheng, Y., 2017. UV-induced molecular signaling differences in melanoma and non-melanoma skin cancer. In: Ahmad, S. (Ed.), Springer. Ultraviolet light in human health, diseases and environment, 1st ed Nottingham. p. 27–40.

[9] Didona, D., Paolino, G., Bottoni, U., Cantisani, C., 2018. Non melanoma skin cancer pathogenesis overview. Biomedicines 6:1–15. https://doi.org/10.3390/biomedicines6010006.

[10] Ceovic, R., Petković, M., Mokos, Z.B., Kostović, K., 2018. Nonsurgical treatment of nonmelanoma skin cancer in the mature patient. Clinics in Dermatology 36:177–187. https://doi.org/10.1016/j.clindermatol.2017.10.009.

[11] Shelton, M.E., Adamson, A.S., 2019. Review and update on evidence-based surgical treatment recommendations for nonmelanoma skin cancer. Dermatologic Clinics 37:425–433. https://doi.org/10.1016/j.det.2019.05.002.

[12] Juarranz, Á., Jaén, P., Sanz-Rodríguez, F., Cuevas, J., González, S., 2008. Photodynamic therapy of cancer basic principles and applications. Clinical and Translational Oncology 10:148–154. https://doi.org/10.1007/s12094-008-0172-2.

[13] Agostinis, P., Berg, K., Cengel, K.A., Foster, T.H., Girotti, A.W., Gollnick, S.O., et al., 2011. Photodynamic therapy of cancer: an update. CA: A Cancer Journal for Clinicians 61:250–281. https://doi.org/10.3322/caac.20114.

[14] Dos Santos, A.F., De Almeida, D.R.Q., Terra, L.F., Baptista, M.S., Labriola, L., 2019. Photodynamic therapy in cancer treatment-an update review. Journal of Cancer Metastasis and Treatment 5:1–20. https://doi.org/10.20517/2394-4722.2018.83.

[15] Ang, J.M., Riaz, I.B., Kamal, M.U., Paragh, G., Zeitouni, N.C., 2017. Photodynamic therapy and pain: a systematic review. Photodiagn Photodyn 19:308–344. https://doi.org/10.1016/j.pdpdt.2017.07.002.

[16] Cohen, D.K., Lee, P.K., 2016. Photodynamic therapy for non-melanoma skin cancers. Cancers 8:90–99. https://doi.org/10.3390/cancers8100090.

[17] Lanoue, J., Goldenberg, G., 2016. Basal Cell carcinoma: a comprehensive review of existing and emerging nonsurgical therapies. The Journal of Clinical and Aesthetic Dermatology 9:26–36. PMID: 27386043.

[18] Casas, A., Di Venosa, G., Hasan, T., Batlle, A., 2011. Mechanisms of resistance to photodynamic therapy. Current Medicinal Chemistry 18:2486–2515. https://doi.org/10.2174/092986711795843272.

[19] Rapozzi, V., Della Pietra, E., Bonavida, B., 2015. Dual roles of nitric oxide in the regulation of tumor cell response and resistance to photodynamic therapy. Redox Biology 6:311–317. https://doi.org/10.1016/j.redox.2015.07.015.

[20] Gracia-Cazaña, T., Salazar, N., Zamarron, A., Mascaraque, M., Lucena, S., Juarranz, A., 2016. Resistance of nonmelanoma skin cancer to nonsurgical treatments. Part II: photodynamic therapy, vismodegib, cetuximab, intralesional methotrexate, and radiotherapy. Actas Dermosifiliogr 107:740–750. https://doi.org/10.1016/j.adengl.2016.08.017.

[21] Olsen, C.E., Weyergang, A., Edwards, V.T., Berg, K., Brech, A., Weisheit, S., et al., 2017. Development of resistance to photodynamic therapy (PDT) in human breast cancer cells is photosensitizer-dependent: possible mechanisms and approaches for overcoming PDT-resistance. Biochemical Pharmacology 144:63–77. https://doi.org/10.1016/j.bcp.2017.08.002.

[22] Rosin, F.C.P., Teixeira, M.G., Pelissari, C., Corrêa, L., 2018. Resistance of oral cancer cells to 5-ALA-mediated photodynamic therapy. Journal of Cellular Biochemistry 119:3554–3562. https://doi.org/10.1002/jcb.26541.

[23] Morandi, A., Indraccolo, S., 2017. Linking metabolic reprogramming to therapy resistance in cancer. Biochimica et Biophysica Acta (BBA) - Reviews on Cancer 1868:1–6. https://doi.org/10.1016/j.bbcan.2016.12.004.

[24] Ma, L., Zong, X., 2020. Metabolic symbiosis in chemoresistance: refocusing the role of aerobic glycolysis. Frontiers in Oncology 10:1–8. https://doi.org/10.3389/fonc.2020.00005.

[25] Warburg, O., 1925. The metabolism of carcinoma cells. The Journal of Cancer Research 9:148–163.

[26] Potter, M., Newport, E., Morten, K.J., 2016. The Warburg effect: 80 years on. Biochemical Society Transactions 44:1499–1505. https://doi.org/10.1158/jcr.1925.148.

[27] Santos, N., Pereira-Nunes, A., Baltazar, F., Granja, S., 2019. Lactate as a regulator of cancer inflammation and immunity. Immunometabolism 1:1–18. https://doi.org/10.20900/immunometab20190015.

[28] Bhattacharya, B., Mohd Omar, M.F., Soong, R., 2018. The Warburg effect and drug resistance. British Journal of Pharmacology 173:970–979. https://doi.org/10.20900/immunometab20190015.

[29] Icard, P., Shulman, S., Farhat, D., Steyaert, J.M., Alifano, M., Lincet, H., 2018. How the Warburg effect supports aggressiveness and drug resistance of cancer cells? Drug Resistance Updates 38:1–11 https://doi.org/10.1016/j.drup.2018.03.001.

[30] Cairns, R.A., Harris, I.S., Mak, T.W., 2011. Regulation of cancer cell metabolism. Nature Reviews Cancer 11:85–95. https://doi.org/10.1038/nrc2981.

[31] Courtnay, R., Ngo, D.C., Malik, N., Ververis, K., Tortorella, S.M., Karagiannis, T.C., 2015. Cancer metabolism and the Warburg effect: the role of HIF-1 and PI3K. Molecular Biology Reports 42:841–851. https://doi.org/10.1007/s11033-015-3858-x.

[32] Kobliakov, V.A., 2019. The mechanisms of regulation of aerobic glycolysis (Warburg effect) by oncoproteins in carcinogenesis. Biochem (Mosc). 84:1117–1128. https://doi.org/10.1134/S0006297919100018.

[33] Wong, N., Ojo, D., Yan, J., Tang, D., 2015. PKM2 contributes to cancer metabolism. Cancer Letters 356:184–191. https://doi.org/10.1016/j.canlet.2014.01.031.

[34] Dayton, T.L., Jacks, T., Vander Heiden, M.G., 2016. PKM2, cancer metabolism, and the road ahead. EMBO Reports 17:1721–1730. https://doi.org/10.15252/embr.201643300.

[35] Wiese, E.K., Hitosugi, T., 2018. Tyrosine kinase signaling in cancer metabolism: PKM2 paradox in the Warburg effect. Frontiers in Cell and Developmental Biology 6:1–8. https://doi.org/10.3389/fcell.2018.00079.

[36] Cuezva, J.M., Ortega, A.D., Willers, I., Sánchez-Cenizo, L., Aldea, M., Sánchez-Aragó, M., 2009. The tumor suppressor function of mitochondria: translation into the clinics. Biochimica et Biophysica Acta 1792:1145–1158. https://doi.org/10.1016/j.bbadis.2009.01.006.

[37] Sánchez-Aragó, M., Formentini, L., Cuezva, J.M., 2013. Mitochondria-mediated energy adaption in cancer: the H+-ATP synthase-geared switch of

metabolism in human tumors. Antioxidants and Redox Signaling 19:285–298. https://doi.org/10.1089/ars.2012.4883.

[38] Esparza-Moltó, P.B., Cuezva, J.M., 2018. The role of mitochondrial H+-ATP synthase in cancer. Frontiers in Oncology 8:1–8. https://doi.org/10.3389/fonc.2018.00053.

[39] Torresano, L., Nuevo-Tapioles, C., Santacatterina, F., Cuezva, J.M., 2020. Metabolic reprogramming and disease progression in cancer patients. Biochimica et Biophysica Acta - Molecular Basis of Disease 165721:1–16. https://doi.org/10.1016/j.bbadis.2020.165721.

[40] Abrahamse, H., Hamblin, M.R., 2016. New photosensitizers for photodynamic therapy. Biochemical Journal 473:347–364. https://doi.org/10.1042/BJ20150942.

[41] Morton, C.A., Szeimies, R.M., Basset-Séguin, N., Calzavara-Pinton, P.G., Gilaberte, Y., Hædersdal, M., et al., 2019. European Dermatology Forum guidelines on topical photodynamic therapy 2019 Part 1: treatment delivery and established indications–actinic keratoses, Bowen's disease and basal cell carcinomas. Journal of the European Academy of Dermatology and Venereology 33:2225–2238. https://doi.org/10.1111/jdv.16017.

[42] Mallik, R., Chowdhury, T.A., 2018. Metformin in cancer. Diabetes Research and Clinical Practice 143:409–419. https://doi.org/10.1016/j.diabres.2018.05.023.

[43] Vancura, A., Bu, P., Bhagwat, M., Zeng, J., Vancurova, I., 2018. Metformin as an anticancer agent. Trends in Pharmacological Sciences 39:867–878. https://doi.org/10.1016/j.tips.2018.07.006.

[44] Osaki, T., Yokoe, I., Takahashi, K., Inoue, K., Ishizuka, M., Tanaka, T., et al., 2017. Metformin enhances the cytotoxicity of 5-aminolevulinic acid-mediated photodynamic therapy in vitro. Oncology Letters 14:1049–1053. https://doi.org/10.3892/ol.2017.6237.

[45] Tudor, D., Nenu, I., Filip, G.A., Olteanu, D., Cenariu, M., Tabaran, F., et al., 2017. Combined regimen of photodynamic therapy mediated by Gallium phthalocyanine chloride and Metformin enhances anti-melanoma efficacy. PLoS One 12:1–23. https://doi.org/10.1371/journal.pone.0173241.

[46] Nenu, I., Popescu, T., Aldea, M.D., Craciun, L., Olteanu, D., Tatomir, C., et al., 2014. Metformin associated with photodynamic therapy–a novel oncological direction. Journal of Photochemistry and Photobiology B 138:80–91. https://doi.org/10.1016/j.jphotobiol.2014.04.027.

[47] Mascaraque, M., Delgado-Wicke, P., Nuevo-Tapioles, C., Gracia-Cazaña, T., Abarca-Lachen, E., González, S., et al., 2020. Metformin as an adjuvant to photodynamic therapy in resistant basal cell carcinoma cells. Cancers 12:668–687. https://doi.org/10.3390/cancers12030668.

[48] Rheinwald, J.G., Beckett, M.A., 1981. Tumorigenic keratinocyte lines requiring anchorage and fibroblast support cultures from human squamous cell carcinomas. Cancer Research 41:1657–1663.

[49] Giard, D.J., Aaronson, S.A., Todaro, G.J., Arnstein, P., Kersey, J.H., Dosik, H., et al., 1973. In vitro cultivation of human tumors: establishment of cell lines derived from a series of solid tumors. Journal of the National Cancer Institute 51:1417–1423. https://doi.org/10.1093/jnci/51.5.1417.

[50] Milla, L.N., Cogno, I.S., Rodríguez, M.E., Sanz-Rodríguez, F., Zamarrón, A., Gilaberte, Y., et al., 2011. Isolation and characterization of squamous carcinoma cells resistant to photodynamic therapy. Journal of Cellular Biochemistry 112:2266–2278.

[51] Adhikary, G., Grun, D., Kerr, C., Balasubramanian, S., Rorke, E.A., Vemuri, M., et al., 2013. Identification of a population of epidermal squamous cell carcinoma cells with enhanced potential for tumor formation. PLoS One 8:1–14. https://doi.org/10.1002/jcb.23145.

[52] Blázquez-Castro, A., Carrasco, E., Calvo, M.I., Jaén, P., Stockert, J.C., Juarranz, Á., et al., 2012. Protoporphyrin IX-dependent photodynamic production of endogenous ROS stimulates cell proliferation. European Journal of Cell Biology 91:216–223. https://doi.org/10.1016/j.ejcb.2011.12.001.

[53] Zakikhani, M., Dowling, R., Fantus, I.G., Sonenberg, N., Pollak, M., 2006. Metformin is an AMP kinase–dependent growth inhibitor for breast cancer cells. Cancer Research 66:10269–10273.

[54] Foucquier, J., Guedj, M., 2015. Analysis of drug combinations: current methodological landscape. Pharmacol Res Perspect 3:1–11. https://doi.org/10.1002/prp2.149.

[55] Dilnawaz, F., Sahoo, S.K., 2013. Enhanced accumulation of curcumin and temozolomide loaded magnetic nanoparticles executes profound cytotoxic effect in glioblastoma spheroid model. European Journal of Pharmaceutics and Biopharmaceutics 85:452–462. https://doi.org/10.1158/0008-5472.

[56] Barrett, M.T., Scheffer, A., Ben-Dor, A., Sampas, N., Lipson, D., Kincaid, R., et al., 2004. Comparative genomic hybridization using oligonucleotide microarrays and total genomic DNA. Proceedings of the National Academy of Sciences of the United States of America 101:17765–17770. https://doi.org/10.1073/pnas.0407979101.

[57] Lucena, S.R., Zamarrón, A., Carrasco, E., Marigil, M.A., Mascaraque, M., Fernández-Guarino, M., et al., 2019. Characterisation of resistance mechanisms developed by basal cell carcinoma cells in response to repeated cycles of photodynamic therapy. Scientific Reports 9:1–15. https://doi.org/10.1038/s41598-019-41313-y.

[58] Hanahan, D., Weinberg, R.A., 2011. Hallmarks of cancer: the next generation. Cell 144:646–674. https://doi.org/10.1016/j.cell.2011.02.013.

[59] Takalkar, A.M., El-Haddad, G., Lilien, D.L., 2008. FDG-PET and PET/CT-Part II. Indian Journal of Radiology and Imaging 18:17–36. https://doi.org/10.4103/0971-3026.38504.

[60] Ashton, T.M., McKenna, W.G., Kunz-Schughart, L.A., Higgins, G.S., 2018. Oxidative phosphorylation as an emerging target in cancer therapy. Clinical Cancer Research 24:2482–2490. https://doi.org/10.1158/1078-0432.

[61] DeBerardinis, R.J., Chandel, N.S., 2020. We need to talk about the Warburg effect. Nature Metabolism 2:127–129. https://doi.org/10.1038/s42255-020-0172-2.

[62] Aspuria, P.J.P., Lunt, S.Y., Väremo, L., Vergnes, L., Gozo, M., Beach, J.A., et al., 2014. Succinate dehydrogenase inhibition leads to epithelial-mesenchymal transition and reprogrammed carbon metabolism. Cancer & Metabolism 2:1–15. https://doi.org/10.1186/2049-3002-2-21.

[63] Guha, M., Srinivasan, S., Raman, P., Jiang, Y., Kaufman, B.A., Taylor, D., et al., 2018. Aggressive triple negative breast cancers have unique molecular signature on the basis of mitochondrial genetic and functional defects. Biochimica et Biophysica Acta - Molecular Basis of Disease 1864:1060–1071. https://doi.org/10.1016/j.bbadis.2018.01.002.

[64] Cuezva, J.M., Krajewska, M., de Heredia, M.L., Krajewski, S., Santamaría, G., Kim, H., et al., 2002. The bioenergetic signature of cancer: a marker of tumor progression. Cancer Research 62:6674–6681.

[65] Najera, L., Alonso-Juarranz, M., Garrido, M., Ballestín, C., Moya, L., Martínez-Díaz, M., et al., 2019. Prognostic implications of markers of the metabolic phenotype in human cutaneous melanoma. British Journal of Dermatology 181:114–127. https://doi.org/10.1111/bjd.17513.

[66] Vallejo, C.G., Cruz-Bermúdez, A., Clemente, P., Hernández-Sierra, R., Garesse, R., Quintanilla, M., 2013. Evaluation of mitochondrial function and metabolic reprogramming during tumor progression in a cell model of skin carcinogenesis. Biochimie 95:1171–1176. https://doi.org/10.1016/j.biochi.2013.01.001.

[67] Cha, P.H., Hwang, J.H., Kwak, D.K., Koh, E., Kim, K.S., Choi, K.Y., 2020. APC loss induces Warburg effect via increased PKM2 transcription in colorectal cancer. British Journal of Cancer 1:1–11. https://doi.org/10.1038/s41416-020-01118-7.

[68] Zhao, Y., Shen, L., Chen, X., Qian, Y., Zhou, Q., Wang, Y., et al., 2015. High expression of PKM2 as a poor prognosis indicator is associated with radiation resistance in cervical cancer. Histology & Histopathology 30:1313–1320. https://doi.org/10.14670/HH-11-627.

[69] Qian, Z., Hu, W., Lv, Z., Liu, H., Chen, D., Wang, Y., et al., 2020. PKM2 upregulation promotes malignancy and indicates poor prognosis for intrahepatic cholangiocarcinoma. Clin Res Hepatol Gastroenterology 44:162–173. https://doi.org/10.1016/j.clinre.2019.06.008.

[70] Zhu, H., Luo, H., Zhu, X., Hu, X., Zheng, L., Zhu, X., 2017. Pyruvate kinase M2 (PKM2) expression correlates with prognosis in solid cancers: a meta-analysis. Oncotarget 8:1628–1640. https://doi.org/10.18632/oncotarget.13703.

[71] Lao-On, U., Attwood, P.V., Jitrapakdee, S., 2018. Roles of pyruvate carboxylase in human diseases: from diabetes to cancers and infection. Journal of Molecular Medicine 96:237–247. https://doi.org/10.1007/s00109-018-1622-0.

[72] Costa, E.C., Moreira, A.F., de Melo-Diogo, D., Gaspar, V.M., Carvalho, M.P., Correia, I.J., 2016. 3D tumor spheroids: an overview on the tools and techniques used for their analysis. Biotechnology Advances 34:1427–1441. https://doi.org/10.1016/j.biotechadv.2016.11.002.

[73] Sant, S., Johnston, P.A., 2017. The production of 3D tumor spheroids for cancer drug discovery. Drug Discovery Today: Technologies 23:27–36. https://doi.org/10.1016/j.ddtec.2017.03.002.

[74] Luo, Q., Hu, D., Hu, S., Yan, M., Sun, Z., Chen, F., 2012. In vitro and in vivo anti-tumor effect of metformin as a novel therapeutic agent in human oral squamous cell carcinoma. BMC Cancer 12:1–10. https://doi.org/10.1186/1471-2407-12-517.

[75] Harada, K., Ferdous, T., Harada, T., Ueyama, Y., 2016. Metformin in combination with 5-fluorouracil suppresses tumor growth by inhibiting the Warburg effect in human oral squamous cell carcinoma. International Journal of Oncology 49:276–284. https://doi.org/10.3892/ijo.2016.3523.

[76] Qi, X., Xu, W., Xie, J., Wang, Y., Han, S., Wei, Z., et al., 2016. Metformin sensitizes the response of oral squamous cell carcinoma to cisplatin treatment through inhibition of NF-κB/HIF-1α signal axis. Scientific Reports 6:35788–35800. https://doi.org/10.1038/srep35788.

[77] Rattan, R., Graham, R.P., Maguire, J.L., Giri, S., Shridhar, V., 2011. Metformin suppresses ovarian cancer growth and metastasis with enhancement of cisplatin cytotoxicity in vivo. Neoplasia 13:483–491. https://doi.org/10.1593/neo.11148.

[78] Li, Y., Wang, M., Zhi, P., You, J., Gao, J.Q., 2018. Metformin synergistically suppress tumor growth with doxorubicin and reverse drug resistance by inhibiting the expression and function of P-glycoprotein in MCF7/ADR cells and xenograft models. Oncotarget 9:2158–2174. https://doi.org/10.18632/oncotarget.23187.

[79] Wang, Y., An, H., Liu, T., Qin, C., Sesaki, H., Guo, S., et al., 2019. Metformin improves mitochondrial respiratory activity through activation of AMPK. Cell Reports 29:1511–1523. https://doi.org/10.1016/j.celrep.2019.09.070.

[80] Izzo, A., Nitti, M., Mollo, N., Paladino, S., Procaccini, C., Faicchia, D., et al., 2017. Metformin restores the mitochondrial network and reverses mitochondrial dysfunction in Down syndrome cells. Human Molecular Genetics 26:1056–1069. https://doi.org/10.1093/hmg/ddx016.

[81] Tyszka-Czochara, M., Bukowska-Strakova, K., Kocemba-Pilarczyk, K.A., Majka, M., 2018. Caffeic acid targets AMPK signaling and regulates tricarboxylic acid cycle anaplerosis while Metformin downregulates HIF-1α-induced glycolytic enzymes in human cervical squamous cell carcinoma lines. Nutrients 10:841–862. https://doi.org/10.3390/nu10070841.

[82] Hu, L., Zeng, Z., Xia, Q., Liu, Z., Feng, X., Chen, J., et al., 2019. Metformin attenuates hepatoma cell proliferation by decreasing glycolytic flux through the HIF-1α/PFKFB3/PFK1 pathway. Life Sciences 239:116966. https://doi.org/10.1016/j.lfs.2019.116966.

[83] Marini, C., Bianchi, G., Buschiazzo, A., Ravera, S., Martella, R., Bottoni, G., et al., 2016. Divergent targets of glycolysis and oxidative phosphorylation result in additive effects of metformin and starvation in colon and breast cancer. Scientific Reports 6:19569–19582. https://doi.org/10.1038/srep19569.

[84] Zhang, H.Y., Zhang, P.N., Sun, H., 2009. Aberration of the PI3K/AKT/mTOR signaling in epithelial ovarian cancer and its implication in cisplatin-based chemotherapy. European Journal of Obstetrics & Gynecology and Reproductive Biology 146:81–86. https://doi.org/10.1016/j.ejogrb.2009.04.035.

[85] Hudson, C.D., Hagemann, T., Mather, S.J., Avril, N., 2014. Resistance to the tyrosine kinase inhibitor axitinib is associated with increased glucose metabolism in pancreatic adenocarcinoma. Cell Death & Disease 5:e1160. https://doi.org/10.1038/cddis.2014.125.

[86] Liu, B., Wang, C., Chen, P., Cheng, B., Cheng, Y., 2018. RACKI induces chemotherapy resistance in esophageal carcinoma by upregulating the PI3K/AKT pathway and Bcl-2 expression. OncoTargets and Therapy 11:211–220. https://doi.org/10.2147/OTT.S152818.

[87] Gremke, N., Polo, P., Dort, A., Schneikert, J., Elmshäuser, S., Brehm, C., et al., 2020. mTOR-mediated cancer drug resistance suppresses autophagy and generates a druggable metabolic vulnerability. Nature Communications 11:1–15. https://doi.org/10.1038/s41467-020-18504-7.

[88] Li, M., Chen, H., Sun, T., Ma, Z., Chen, X., Wu, D., et al., 2020. p70S6K promotes acquired resistance of erlotinib through induction of epithelial-mesenchymal transition in non-small cell lung carcinoma. OncoTargets and Therapy 13:5257–5270. https://doi.org/10.2147/OTT.S249695.

[89] Ma, B.B., Lui, V.W., Hui, E.P., Lau, C.P., Ho, K., Ng, M.H., et al., 2010. The activity of mTOR inhibitor RAD001 (everolimus) in nasopharyngeal carcinoma and cisplatin-resistant cell lines. Investigational New Drugs 28:413–420. https://doi.org/10.1007/s10637-009-9269-x.

[90] Emmanouilidi, A., Falasca, M., 2017. Targeting PDK1 for chemosensitization of cancer cells. Cancers 9:140–165. https://doi.org/10.3390/cancers9100140.

[91] Wang, H.J., Yang, Z.X., Dai, X.T., Chen, Y.F., Yang, H.P., Zhou, X.D., 2017. Bisdemethoxycurcumin sensitizes cisplatin-resistant lung cancer cells to chemotherapy by inhibition of CA916798 and PI3K/AKT signaling. Apoptosis 22:1157–1168. https://doi.org/10.3390/cancers9100140.

[92] Alipour, F., Riyahi, N., Safaroghli-Azar, A., Sari, S., Zandi, Z., Bashash, D., 2019. Inhibition of PI3K pathway using BKM120 intensified the chemosensitivity of breast cancer cells to arsenic trioxide (ATO). The International Journal of Biochemistry & Cell Biology 116:105615–105625. https://doi.org/10.1016/j.biocel.2019.105615.

[93] Honjo, S., Ajani, J.A., Scott, A.W., Chen, Q., Skinner, H.D., Stroehlein, J., et al., 2014. Metformin sensitizes chemotherapy by targeting cancer stem cells and the mTOR pathway in esophageal cancer. International Journal of Oncology 45:567–574. https://doi.org/10.3892/ijo.2014.2450.

[94] Rocha, G.Z., Dias, M.M., Ropelle, E.R., Osório-Costa, F., Rossato, F.A., Vercesi, A.E., et al., 2011. Metformin amplifies chemotherapy-induced AMPK activation and antitumoral growth. Clinical Cancer Research 17:3993–4005. https://doi.org/10.1158/1078-0432.

